

A higher order polyhedral method for contact mechanics with Tresca friction

Jérôme Droniou^{1,2}, Raman Kumar¹, Roland Masson³, and Ritesh Singla¹

¹IMAG, Univ. Montpellier, CNRS, Montpellier, France, jerome.droniou@cnrs.fr, raman.kumar@umontpellier.fr, iritesh281@gmail.com

²School of Mathematics, Monash University, Melbourne, Australia

³Université Côte d'Azur, Inria, CNRS, Laboratoire J.A. Dieudonné, Team Galets, Nice, France, roland.masson@univ-cotedazur.fr

April 8, 2026

Abstract

In this work, we design and analyze a Discrete de Rham (DDR) scheme for a contact mechanics problem involving fractures along which a model of Tresca friction is considered. Our approach is based on a mixed formulation involving a displacement field and a Lagrange multiplier, enforcing the contact conditions, representing tractions at fractures. The approximation space for the displacement is made of vectors values attached to each vertex, edge, face, and element, while the Lagrange multiplier space is approximated by piecewise constant vectors on each fracture face. The displacement degrees of freedom allow reconstruct piecewise quadratic approximations of this field. We prove a discrete Korn inequality that account for the fractures, as well as an inf-sup condition (in a non-standard $H^{-1/2}$ -norm) between the discrete Lagrange multiplier space and the discrete displacement space. We provide an in-depth error analysis of the scheme and show that, contrary to usual low-order nodal-based schemes, our method is robust in the quasi-incompressible limit for the primal variable (displacement). An extensive set of numerical experiments confirms the theoretical analysis and demonstrate the practical accuracy and robustness of the scheme.

Key words. Contact-mechanics, fracture networks, Discrete de Rham complex, discrete inf-sup condition, discrete Korn inequality, error estimates, polyhedral method.

MSC2020. 65N30, 65N15

1 Introduction

The study of Contact mechanics in fractured porous media plays a crucial role in subsurface applications where understanding the complex interplay between mechanical deformation, fracture behavior, and fluid flow is essential for accurate prediction and risk assessment. A prime example of this is CO₂ sequestration, where the action of injecting the gas can create a buildup of pressure that may eventually cause the reactivation of faults by changing pore pressure and normal stress on fracture surfaces, thus posing risks of deformation of rocks, CO₂ leakage [1] and seismic activity [35]. Fractures are classically represented as a network of planar surfaces connected to the surrounding matrix domain, resulting in mixed-dimensional models that have been extensively studied in poromechanics [1, 7, 8, 10, 9, 34, 35, 36, 44]. The movement along fractures is governed by nonlinear frictional laws arising from inequality constraints imposed by non-penetration conditions and the non-smooth nature of friction laws. The Tresca friction

model, which prescribes a yield threshold for tangential traction independent of normal traction, provides a mathematically tractable framework while capturing essential friction behavior [14]. More generally, the Coulomb friction law, where the tangential traction threshold depends on the normal stress, better represents physical friction but introduces additional nonlinearity [13].

Capturing the geometric complexity of fracture networks with their corners and intersections typically requires a robust and accurate discretization method. Traditional finite element methods (FEM), while well-established for regular meshes, often struggle with non-simplicial element shapes that naturally arise in geological applications [11, 25]. This challenge has motivated the development of polytopal discretization methods offering greater geometric flexibility while maintaining accuracy and stability. Several families of polytopal methods have emerged in computational mechanics over the past two decades, including Hybrid High Order (HHO) [20, 25], Discontinuous Galerkin [38], Virtual Element Methods (VEM) [5], and the Discrete De Rham (DDR) method [24, 26]. Some of these have been extended to account for contact mechanics, such as: VEM on non-conforming meshes [18], HHO combined with Nitsche’s contact formulation [16], VEM for Nitsche frictionless contact [42] and Coulomb frictional contact mechanics [41], and VEM with bubble stabilisation [32]. So far, DDR has not been considered for contact mechanics, but it is a natural candidate for mechanics problems since it provides a nodal-based discrete version of the H^1 space; it moreover already proved efficient in approximating solid and fluid mechanics models, including Navier-Stokes equations [21], Maxwell equations on manifolds [29], Yang-Mills equations [30], as well as the Reissner-Mindlin and Kirchoff-Love plate problems [22, 23].

The discretization of contact mechanics has been an active area of research, driven by the challenges of variational inequalities, the nonlinearity of the frictional constraints, and the need to ensure stability under unilateral conditions. For mixed-dimensional models with fractures represented as co-dimension one manifolds (e.g., 2D surfaces in a 3D medium), additional complexities arise due to intersections, corners, and tips. The mixed-dimensional framework for flow in fractured porous media was pioneered in [43, 3], in which discrete fracture-matrix (DFM) models are developed to represent fractures as lower-dimensional manifolds embedded in the porous matrix. In mixed formulation with Lagrange multipliers, surface tractions are introduced as independent unknowns, with the Lagrange multiplier representing the traction at the contact interface, and enforcing dual cone constraint [12, 2]. A fundamental requirement for well-posedness is the satisfaction of a discrete inf-sup condition between displacement and multiplier spaces. [6] introduced the \mathbb{P}_1 -bubble FEM discretization for the Signorini problem, enriching the displacement space with bubble functions to satisfy the inf-sup condition. In the polytopal framework, the recent work of [32] extended the bubble-stabilized mixed formulation to the first-order VEM framework for contact mechanics with Tresca friction. Furthermore, [45] proposed an abstract framework for the *priori* error analysis of 3D frictionless contact problems using quadratic finite elements. They established an $\mathcal{O}(h^{\frac{1}{2}+\nu})$ convergence for $\frac{1}{2} < \nu < 1$, when the solution belongs to $H^{\frac{3}{2}+\nu}$, providing H^1 and $H^{-1/2}$ -norm bounds for displacement and traction errors, respectively. The analysis assumes constant normal vectors and no friction, together with an additional regularity condition [45, Assumption 4] on the contact zone (where the transition between contact and non-contact occurs) to ensure smooth behavior near the interface. It is noted that the estimates are not robust for nearly incompressible materials (that is, when the Poisson ratio tends to 0.5).

In this work, we design and analyze a second-order DDR scheme for contact mechanics with Tresca friction on fracture networks modeled with co-dimension 1 interfaces. In the discrete formulation, the displacement field is approximated using vector values attached to vertices, edges, faces, and elements, and the contact constraints are enforced through face-wise constant La-

grange multipliers on the fracture network. The chosen degrees of freedom for the displacement allow us to reconstruct piecewise quadratic displacements on the edges, faces, and elements. A key analytical result of this study is the discrete Korn inequality adapted to the DDR-type spaces, where our proof draws inspiration from [32] but differs substantially due to the presence of quadratic face displacement reconstruction. Furthermore, we establish a discrete inf-sup condition based on a non-standard $H^{-1/2}$ -type norm on the fracture network, ensuring stability of the mixed formulation. We provide a comprehensive error analysis for solutions with $H^{\frac{3}{2}+\tau}$ regularity, which yields an $\mathcal{O}(h^{\frac{1}{2}+\tau})$, where h is the mesh size, order convergence in the energy norm (for $0 < \tau < 1$ when the Tresca threshold vanishes and $0 < \tau \leq 1/2$ otherwise – although the numerical results suggests that $0 < \tau < 1$ remains valid even when the Tresca threshold does not vanish). Moreover, the error estimates are robust for the primal variable (displacement) in the incompressible limit, when the Poisson ratio tends to $\frac{1}{2}$. This is made possible by the use of a bespoke interpolator (designed by correcting the cell values of the standard DDR interpolator) that enjoys a commutation (Fortin) property with the continuous and discrete divergences. While the global $H^{\frac{3}{2}+\tau}$ regularity assumption is standard for establishing optimal convergence rates in contact problems, realistic fracture network configurations may exhibit reduced regularity near fracture tips and intersections [19]. This could be dealt with by incorporating locally weighted regularity estimates that represent an interesting direction for future theoretical developments out of the scope of the present work. We also note that, although the analysis is presented for a Tresca-type friction model, the extension of the proposed discretisation to the more involved case of Coulomb friction can be carried out without difficulty, following the same approach as for the lowest-order scheme in [31]. However, very few error estimates have been derived in the Coulomb case with non-penetration, all based on a mesh-dependent smallness assumption on the friction coefficient [40]. A more tractable extension to be investigated would consist in considering a normal compliance model with Coulomb friction, following the approach proposed in [46].

The rest of this paper is organized as follows. Section 2 introduces the governing equations for contact with Tresca friction, presenting the strong and weak formulations. Section 3 details the DDR discretization, including mesh notation (Section 3.1), the construction of discrete spaces with degrees of freedom (Section 3.2), displacement and gradient reconstruction (Section 3.3), and the discrete scheme (Section 3.4) including its well posedness. Section 4 states the main results, starting from an abstract error estimate (Theorem 4.2) that does not assume any regularity on the solution, before presenting an error estimate (Theorem 4.3) providing rates of convergence depending on the regularity of the solution; the proofs are presented in Section 5. Finally, the theoretical results are validated by extensive numerical tests presented in Section 6.

2 Model

We consider a discrete fracture-matrix model on the polyhedral domain $\Omega \subset \mathbb{R}^3$ including a fracture network Γ with co-dimension 1 defined as the union of flat fractures Γ_i :

$$\bar{\Gamma} = \bigcup_{i \in \mathbf{I}} \bar{\Gamma}_i.$$

We assume that Γ does not disconnect any part of Ω from $\partial\Omega$, that is, the boundary of each connected component of $\Omega \setminus \Gamma$ contains a portion of $\partial\Omega$ of non-zero $(d-1)$ -dimensional measure. Each fracture Γ_i (for $i \in \mathbf{I}$) is a polygonal simply connected open subdomain of a plane of \mathbb{R}^3 . Without restriction of generality, it is assumed that fractures may only intersect at their boundaries. The two sides of a given fracture of Γ are denoted by \pm in the matrix domain $\Omega \setminus \bar{\Gamma}$,

and respectively called positive and negative sides. The two unit normal vectors \mathbf{n}^\pm , oriented outward from the sides \pm , satisfy $\mathbf{n}^+ + \mathbf{n}^- = \mathbf{0}$. For simplicity, given homogeneous Dirichlet boundary conditions, the space

$$\mathbf{U}_0 := H_0^1(\Omega \setminus \bar{\Gamma})^3$$

of the displacements (which may be discontinuous across fractures) is endowed with the norm $\|\mathbf{v}\|_{H^1(\Omega \setminus \bar{\Gamma})} = \|\nabla \mathbf{v}\|_{L^2(\Omega \setminus \bar{\Gamma})}$. The oriented jump operator on Γ for functions $\mathbf{u} \in \mathbf{U}_0$ is defined by

$$[[\mathbf{u}]] := \gamma^+ \mathbf{u} - \gamma^- \mathbf{u},$$

where γ^\pm are the trace operators on each side of Γ . Its normal and tangential components are denoted respectively by $[[\mathbf{u}]]_{\mathbf{n}} := [[\mathbf{u}]] \cdot \mathbf{n}^+$ and $[[\mathbf{u}]]_{\tau} := [[\mathbf{u}]] - [[\mathbf{u}]]_{\mathbf{n}} \mathbf{n}^+$. The normal trace operators on $H_{\text{div}}(\Omega \setminus \bar{\Gamma})$ are denoted by $\gamma_{\mathbf{n}}^\pm$. The symmetric gradient operator $\boldsymbol{\epsilon}$ is defined on \mathbf{U}_0 by $\boldsymbol{\epsilon}(\mathbf{v}) := \frac{1}{2}(\nabla \mathbf{v} + (\nabla \mathbf{v})^t)$.

The model we consider accounts for the mechanical equilibrium equation with a linear isotropic elastic constitutive law and a Tresca frictional contact model at matrix-fracture interfaces. In its strong form, it is written

$$\begin{cases} -\operatorname{div} \boldsymbol{\sigma}(\mathbf{u}) = \mathbf{f} & \text{on } \Omega \setminus \bar{\Gamma}, \\ \boldsymbol{\sigma}(\mathbf{u}) = \frac{E}{1+\nu} \left(\boldsymbol{\epsilon}(\mathbf{u}) + \frac{\nu}{1-2\nu} (\operatorname{tr} \boldsymbol{\epsilon}(\mathbf{u})) \mathbf{I}_3 \right) & \text{on } \Omega \setminus \bar{\Gamma}, \\ \gamma_{\mathbf{n}}^+ \boldsymbol{\sigma}(\mathbf{u}) + \gamma_{\mathbf{n}}^- \boldsymbol{\sigma}(\mathbf{u}) = \mathbf{0} & \text{on } \Gamma, \\ T_{\mathbf{n}}(\mathbf{u}) \leq 0, [[\mathbf{u}]]_{\mathbf{n}} \leq 0, [[\mathbf{u}]]_{\mathbf{n}} T_{\mathbf{n}}(\mathbf{u}) = 0 & \text{on } \Gamma, \\ |\mathbf{T}_{\tau}(\mathbf{u})| \leq g & \text{on } \Gamma, \\ \mathbf{T}_{\tau}(\mathbf{u}) \cdot [[\mathbf{u}]]_{\tau} + g |[[\mathbf{u}]]_{\tau} | = 0 & \text{on } \Gamma, \end{cases} \quad (2.1)$$

with a Tresca threshold $g \geq 0$, Poisson ratio ν , and Young's modulus E satisfying $\frac{E}{1+\nu} \in [\mu_1, \mu_2]$ with $0 < \mu_1 \leq \mu_2$, the 3×3 identity matrix \mathbf{I}_3 , and normal and tangential surface tractions $T_{\mathbf{n}}(\mathbf{u}) = \gamma_{\mathbf{n}}^+ \boldsymbol{\sigma}(\mathbf{u}) \cdot \mathbf{n}^+$ and $\mathbf{T}_{\tau}(\mathbf{u}) = \gamma_{\mathbf{n}}^+ \boldsymbol{\sigma}(\mathbf{u}) - T_{\mathbf{n}}(\mathbf{u}) \mathbf{n}^+$. We assume henceforth that the external force term \mathbf{f} belongs to $L^2(\Omega)^3$ and that $g \in L^2(\Gamma)$ is nonnegative.

The weak formulation of the mechanical model with Tresca frictional-contact (2.1) is written in mixed form using a vector-valued Lagrange multiplier $\boldsymbol{\lambda}: \Gamma \rightarrow \mathbb{R}^3$ at matrix-fracture interfaces. Define the displacement jump space by

$$\mathbf{W}_j(\Gamma) := \{[[\mathbf{v}]] : \mathbf{v} \in \mathbf{U}_0\}$$

and denote by $\mathbf{W}'_j(\Gamma)$ its dual space; the duality pairing between these two spaces is written $\langle \cdot, \cdot \rangle_{\Gamma}$. We note that $L^2(\Gamma)^3 \subset \mathbf{W}'_j(\Gamma)$ and that $\langle \boldsymbol{\mu}, \mathbf{v} \rangle_{\Gamma} := \int_{\Gamma} \boldsymbol{\mu} \cdot \mathbf{v}$ whenever $\boldsymbol{\mu} \in L^2(\Gamma)^3$. The dual cone is then defined by

$$\mathcal{C}_f := \left\{ \boldsymbol{\mu} \in \mathbf{W}'_j(\Gamma) : \langle \boldsymbol{\mu}, \mathbf{v} \rangle_{\Gamma} \leq \int_{\Gamma} g |\mathbf{v}_{\tau}| \text{ for all } \mathbf{v} \in \mathbf{W}_j(\Gamma) \text{ with } \mathbf{v} \cdot \mathbf{n}^+ \leq 0 \right\}.$$

The weak mixed-variational formulation of (2.1) reads: find $\mathbf{u} \in \mathbf{U}_0$ and $\boldsymbol{\lambda} \in \mathcal{C}_f$ such that

$$\begin{aligned} \int_{\Omega} \boldsymbol{\sigma}(\mathbf{u}) : \boldsymbol{\epsilon}(\mathbf{v}) + \langle \boldsymbol{\lambda}, [[\mathbf{v}]] \rangle_{\Gamma} &= \int_{\Omega} \mathbf{f} \cdot \mathbf{v} & \forall \mathbf{v} \in \mathbf{U}_0, \\ \langle \boldsymbol{\mu} - \boldsymbol{\lambda}, [[\mathbf{u}]] \rangle_{\Gamma} &\leq 0 & \forall \boldsymbol{\mu} \in \mathcal{C}_f. \end{aligned} \quad (2.2a)$$

We can see from this formulation that $\boldsymbol{\lambda} = -\gamma_{\mathbf{n}}^+ \boldsymbol{\sigma}(\mathbf{u}) = \gamma_{\mathbf{n}}^- \boldsymbol{\sigma}(\mathbf{u})$.

3 Scheme

3.1 Mesh

We take a polyhedral mesh of the domain Ω that is compliant with the fracture network Γ , and we assume that the Tresca threshold g is piecewise constant on the trace \mathcal{F}_Γ of the mesh on Γ . By compliance,

$$\bar{\Gamma} = \bigcup_{\sigma \in \mathcal{F}_\Gamma} \bar{\sigma}.$$

The set of cells K , the set of faces σ , the set of edges e and the set of vertices s are denoted respectively by \mathcal{M} , \mathcal{F} , \mathcal{E} and \mathcal{V} . For $z \in \mathcal{M} \cup \mathcal{F} \cup \mathcal{E}$, we denote by h_z the diameter of z and by $|z|$ its measure (in its own dimension). We also set $h = \max_{K \in \mathcal{M}} h_K$. For $\mathcal{X} \in \{\mathcal{M}, \mathcal{F}, \mathcal{E}, \mathcal{V}\}$ and $z \in \mathcal{M} \cup \mathcal{F} \cup \mathcal{E} \cup \mathcal{V}$, \mathcal{X}_z denotes the set of entities in \mathcal{X} that have z in their boundary or that belong to the boundary of z . So, for example, the set of faces in the boundary of some $K \in \mathcal{M}$ is written \mathcal{F}_K , and the set of cells having a vertex $s \in \mathcal{V}$ in their boundary is \mathcal{M}_s . If $\mathcal{X} \in \{\mathcal{F}, \mathcal{E}, \mathcal{V}\}$ we denote by \mathcal{X}^{int} the set of elements of \mathcal{X} that lie in Ω and by \mathcal{X}^{ext} those that lie on $\partial\Omega$.

In the following, we write $a \lesssim b$ as shorthand for $a \leq Cb$ for some constant C that may depend on Ω , the mesh regularity parameter and the Young modulus E , but does not depend on the Poisson ratio ν or the mesh size h . In particular, the constant C does not blow up as $\nu \rightarrow \frac{1}{2}$ (quasi-incompressible regime).

Next, we introduce the broken Sobolev space $H^1(\mathcal{M})$ as

$$H^1(\mathcal{M}) := \{v \in L^2(\Omega) : v|_K \in H^1(K) \quad \forall K \in \mathcal{M}\}.$$

For any $\sigma \in \mathcal{F}^{\text{int}}$, we denote $\sigma = K|L$ where K and L are the two cells that share the face σ . For a given cell $K \in \mathcal{M}$ and a face $\sigma \in \mathcal{F}_K$, let $\mathbf{n}_{K\sigma}$ represent the unit outward normal to K on σ . Additionally, for a face $\sigma \in \mathcal{F}$ and an edge $e \in \mathcal{E}_\sigma$, we denote by $\mathbf{n}_{\sigma e}$ the unit outward normal to σ , in the plane spanned by this face, along the edge e .

If $X \in \mathcal{M} \cup \mathcal{F} \cup \mathcal{E}$ and $l \in \mathbb{N}$, the space of polynomials of degree $\leq l$ on X is denoted by $\mathbb{P}^l(X)$. The $L^2(X)^3$ -orthogonal projection on $\mathbb{P}^l(X)^3$ is written Π_X^l and $L^2(X)^{3 \times 3}$ -orthogonal projection on $\mathbb{P}^l(X)^{3 \times 3}$ is denoted as $\mathbf{\Pi}_X^l$. In case $\mathcal{X} = \mathcal{M}$ or $\mathcal{X} = \mathcal{F}_\Gamma$, the notation $\mathbb{P}^l(\mathcal{X})$ denotes the space of piecewise polynomials of degree at most l on \mathcal{X} .

3.2 Spaces

To account for the discontinuity of the discrete displacement field at matrix-fracture interfaces, the displacement degrees of freedom (DOFs) can be discontinuous across the fracture network; they are however continuous across mesh elements not on this network. To represent this, for each face, edge or vertex $z \in \mathcal{F} \cup \mathcal{E} \cup \mathcal{V}$ and each cell $K \in \mathcal{M}_z$ containing z , we denote by $\mathcal{K}z$ the set of cells containing z and on the same side of K with respect to the fracture network. For two cells $K, L \in \mathcal{M}_z$, we have $\mathcal{K}z = \mathcal{L}z$ if and only if K, L are on the same side of Γ . We then denote by $\mathbf{v}_{\mathcal{K}z}$ the displacement unknown at the face/edge/vertex z corresponding to the side K in the matrix; the discussion above shows that if L is on the same side of Γ as K then $\mathbf{v}_{\mathcal{K}z} = \mathbf{v}_{\mathcal{L}z}$; however, if K, L lie on different sides, then $\mathbf{v}_{\mathcal{K}z}$ and $\mathbf{v}_{\mathcal{L}z}$ are independent, which represents the possible discontinuity of the displacement across fractures. Note that if z does

not lie on Γ , then $\mathcal{K}z = \mathcal{M}_z$ and there is a unique displacement unknown at z (still denoted by $\mathbf{v}_{\mathcal{K}z}$), which represents the continuity of the displacement outside fractures.

Taking into account these multiple DOFs on fracture entities, the numerical scheme for (2.2) is based on the vector-valued version of the $X_{\mathbf{grad},h}^1$ space of the Discrete De Rham complex [26]. This scheme is a higher-order extension of the one proposed in [31, 32]. The global discrete space is defined as:

$$\mathbf{X}_{\mathbf{grad},h} := \{ \underline{\mathbf{v}}_h = ((\mathbf{v}_{\mathcal{K}s})_{K \in \mathcal{M}, s \in \mathcal{V}_K}, (\mathbf{v}_{\mathcal{K}e})_{K \in \mathcal{M}, e \in \mathcal{E}_K}, (\mathbf{v}_{\mathcal{K}\sigma})_{K \in \mathcal{M}, \sigma \in \mathcal{F}_K}, (\mathbf{v}_K)_{K \in \mathcal{M}}) : \mathbf{v}_{\mathcal{K}s} \in \mathbb{R}^3, \mathbf{v}_{\mathcal{K}e} \in \mathbb{R}^3, \mathbf{v}_{\mathcal{K}\sigma} \in \mathbb{R}^3, \text{ and } \mathbf{v}_K \in \mathbb{R}^3 \},$$

and its subspace incorporating homogeneous Dirichlet boundary conditions on $\partial\Omega$ is

$$\mathbf{X}_{\mathbf{grad},h,0} := \{ \underline{\mathbf{v}}_h \in \mathbf{X}_{\mathbf{grad},h} : \mathbf{v}_{\mathcal{K}s} = 0 \text{ if } s \in \mathcal{V}^{\text{ext}}, \mathbf{v}_{\mathcal{K}e} = 0 \text{ if } e \in \mathcal{E}^{\text{ext}}, \mathbf{v}_{\mathcal{K}\sigma} = 0 \text{ if } \sigma \in \mathcal{F}^{\text{ext}} \}.$$

For each $K \in \mathcal{M}$, the local discrete space gathers the components attached to a cell, its faces, edges and vertices.

$$\mathbf{X}_{\mathbf{grad},K} := \{ \underline{\mathbf{v}}_K = ((\mathbf{v}_{\mathcal{K}s})_{s \in \mathcal{V}_K}, (\mathbf{v}_{\mathcal{K}e})_{e \in \mathcal{E}_K}, (\mathbf{v}_{\mathcal{K}\sigma})_{\sigma \in \mathcal{F}_K}, \mathbf{v}_K) : \mathbf{v}_{\mathcal{K}s} \in \mathbb{R}^3, \mathbf{v}_{\mathcal{K}e} \in \mathbb{R}^3, \mathbf{v}_{\mathcal{K}\sigma} \in \mathbb{R}^3, \text{ and } \mathbf{v}_K \in \mathbb{R}^3 \},$$

The Lagrange multiplier plays the role of approximations of $-\gamma_{\mathbf{n}}^+(\mathbf{u})$. Its space is made of piecewise constant vectors:

$$\mathbf{M}_h := \{ \boldsymbol{\lambda}_h \in L^2(\Gamma)^3 : \boldsymbol{\lambda}_\sigma := (\boldsymbol{\lambda}_h)|_\sigma \text{ is a constant } \forall \sigma \in \mathcal{F}_\Gamma \}.$$

The normal and tangential components of $\boldsymbol{\lambda}_h \in \mathbf{M}_h$ are

$$\lambda_{h,\mathbf{n}} = \boldsymbol{\lambda}_h \cdot \mathbf{n}^+, \quad \boldsymbol{\lambda}_{h,\tau} = \boldsymbol{\lambda}_h - \lambda_{h,\mathbf{n}} \mathbf{n}^+,$$

and the discrete dual cone is

$$\mathcal{C}_{f,h} := \{ \boldsymbol{\lambda}_h \in \mathbf{M}_h : \lambda_{h,\mathbf{n}} \geq 0, |\boldsymbol{\lambda}_{h,\tau}| \leq g \} \subset \mathcal{C}_f.$$

3.3 Gradient and Reconstruction Operators

For each edge $e \in \mathcal{E}_K$, define the local edge reconstruction as $\Upsilon_{Ke}^2 : \mathbf{X}_{\mathbf{grad},h,0} \rightarrow \mathbb{P}^2(e)^3$ such that

$$\Upsilon_{Ke}^2 \underline{\mathbf{v}}_h(\mathbf{x}_s) = \mathbf{v}_{\mathcal{K}s} \quad \forall s \in \mathcal{V}_e, \quad \text{and} \quad \Pi_e^0 \Upsilon_{Ke}^2 \underline{\mathbf{v}}_h = \mathbf{v}_{\mathcal{K}e}.$$

Next, for any face $\sigma \in \mathcal{F}_K$ we introduce the local face gradient reconstruction $\mathbb{G}_{K\sigma}^1 : \mathbf{X}_{\mathbf{grad},h,0} \rightarrow \mathbb{P}^1(\sigma)^{3 \times 2}$ and face displacement reconstruction $\Upsilon_{K\sigma}^2 : \mathbf{X}_{\mathbf{grad},h,0} \rightarrow \mathbb{P}^2(\sigma)^3$ in the following manner: for all $\boldsymbol{\xi} \in \mathbb{P}^1(\sigma)^{3 \times 2}$ and $\boldsymbol{\eta} \in \mathbb{Z}(\sigma)^3 := [(\mathbf{x} - \bar{\mathbf{x}}_\sigma) \mathbb{P}^2(\sigma)]^3$,

$$\int_\sigma \mathbb{G}_{K\sigma}^1 \underline{\mathbf{v}}_h : \boldsymbol{\xi} = - \int_\sigma \mathbf{v}_{\mathcal{K}\sigma} \cdot \text{div}(\boldsymbol{\xi}) + \sum_{e \in \mathcal{E}_\sigma} \int_e \Upsilon_{Ke}^2 \underline{\mathbf{v}}_h \cdot \boldsymbol{\xi} \mathbf{n}_{\sigma e},$$

and

$$\int_\sigma \Upsilon_{K\sigma}^2 \underline{\mathbf{v}}_h \cdot \text{div}(\boldsymbol{\eta}) = - \int_\sigma \mathbb{G}_{K\sigma}^1 \underline{\mathbf{v}}_h : \boldsymbol{\eta} + \sum_{e \in \mathcal{E}_\sigma} \int_e \Upsilon_{Ke}^2 \underline{\mathbf{v}}_h \cdot \boldsymbol{\eta} \mathbf{n}_{\sigma e}, \quad (3.1)$$

where $\mathbb{Z}(\sigma)^3$ is identified with a space of matrix-valued functions (with independent copies of $(\mathbf{x} - \bar{\mathbf{x}}_\sigma) \mathbb{P}^2(\sigma)$ on each row), $\bar{\mathbf{x}}_\sigma$ is the barycenter of face σ , and the divergences of matrices are

taken row-wise. When writing $\mathbb{G}_{K\sigma}^1 \mathbf{v}_h$ and $\boldsymbol{\xi}$ above as 3×2 -matrices, we actually consider that each row of this matrix is tangent to σ (which gives meaning to $\operatorname{div}(\boldsymbol{\xi})$, the divergence being in the coordinate system on σ); likewise, each copy of $\mathbb{Z}(\sigma)$ in $\mathbb{Z}(\sigma)^3$ is interpreted as a space of tangent polynomials to σ , and $\mathbb{Z}(\sigma)^3$ as a space of 3×2 polynomial-valued matrices. Note also that (3.1) uniquely defines $\Upsilon_{K\sigma}^2$ because $\operatorname{div} : \mathbb{Z}(\sigma) \rightarrow \mathbb{P}^2(\sigma)$ is an isomorphism [4, Corollary 7.3].

Let $\sigma \in \mathcal{F}_\Gamma$ be a fracture face, and let K, L be the two cells on each side of σ , with K lying on the positive side of σ (that is, \mathbf{n}^+ introduced in Section 2 is the outer normal to K on σ). We define the displacement jump operator on σ as $[[\cdot]]_\sigma : \mathbf{X}_{\mathbf{grad},h,0} \rightarrow \mathbb{P}^2(\sigma)^3$ such that, for all $\mathbf{v}_h \in \mathbf{X}_{\mathbf{grad},h,0}$,

$$[[\mathbf{v}_h]]_\sigma := \Upsilon_{K\sigma}^2 \mathbf{v}_h - \Upsilon_{L\sigma}^2 \mathbf{v}_h. \quad (3.2)$$

Next, for any element $K \in \mathcal{M}$, we introduce the local element gradient reconstruction $\mathbb{G}_K^1 : \mathbf{X}_{\mathbf{grad},h,0} \rightarrow \mathbb{P}^1(K)^{3 \times 3}$ and element displacement reconstruction $\Upsilon_K^2 : \mathbf{X}_{\mathbf{grad},h,0} \rightarrow \mathbb{P}^2(K)^3$ in the following manner: for all $\boldsymbol{\xi} \in \mathbb{P}^1(K)^{3 \times 3}$ and $\boldsymbol{\eta} \in \mathbb{Z}(K)^3 := [(\mathbf{x} - \bar{\mathbf{x}}_K)\mathbb{P}^2(K)]^3$,

$$\int_K \mathbb{G}_K^1 \mathbf{v}_h : \boldsymbol{\xi} = - \int_K \mathbf{v}_K \cdot \operatorname{div}(\boldsymbol{\xi}) + \sum_{\sigma \in \mathcal{F}_K} \int_\sigma \Upsilon_{K\sigma}^2 \mathbf{v}_h \cdot \boldsymbol{\xi} \mathbf{n}_{K\sigma}, \quad (3.3)$$

and

$$\int_K \Upsilon_K^2 \mathbf{v}_h \cdot \operatorname{div}(\boldsymbol{\eta}) = - \int_K \mathbb{G}_K^1 \mathbf{v}_h : \boldsymbol{\eta} + \sum_{\sigma \in \mathcal{F}_K} \int_\sigma \Upsilon_{K\sigma}^2 \mathbf{v}_h \cdot \boldsymbol{\eta} \mathbf{n}_{K\sigma}$$

(with the same considerations for $\mathbb{Z}(K)^3$ and divergence of matrices as above). Here, $\bar{\mathbf{x}}_K$ is the barycenter for each cell K .

These local jump, gradient and displacement reconstructions are patched together to create their global piecewise polynomial counterparts $[[\cdot]]_h : \mathbf{X}_{\mathbf{grad},h,0} \rightarrow \mathbb{P}^2(\mathcal{F}_\Gamma)^3$, $\mathbb{G}_h^1 : \mathbf{X}_{\mathbf{grad},h,0} \rightarrow \mathbb{P}^1(\mathcal{M})^{3 \times 3}$, and $\Upsilon_h^2 : \mathbf{X}_{\mathbf{grad},h,0} \rightarrow \mathbb{P}^2(\mathcal{M})^3$: for all $\mathbf{v}_h \in \mathbf{X}_{\mathbf{grad},h,0}$,

$$\begin{aligned} ([[\mathbf{v}_h]])|_\sigma &= [[\mathbf{v}_h]]_\sigma & \forall \sigma \in \mathcal{F}_\Gamma, \\ (\mathbb{G}_h^1 \mathbf{v}_h)|_K &= \mathbb{G}_K^1 \mathbf{v}_h & \forall K \in \mathcal{M}, \\ (\Upsilon_h^2 \mathbf{v}_h)|_K &= \Upsilon_K^2 \mathbf{v}_h & \forall K \in \mathcal{M}. \end{aligned}$$

3.4 Discrete Formulation

Define the discrete symmetric gradient $\boldsymbol{\epsilon}_h$, divergence div_h , and stress tensor $\boldsymbol{\sigma}_h$ as: for all $\mathbf{v}_h \in \mathbf{X}_{\mathbf{grad},h}$,

$$\begin{aligned} \boldsymbol{\epsilon}_h(\mathbf{v}_h) &:= \frac{1}{2}(\mathbb{G}_h^1 \mathbf{v}_h + (\mathbb{G}_h^1 \mathbf{v}_h)^T), \quad \operatorname{div}_h(\mathbf{v}_h) := \operatorname{tr}(\boldsymbol{\epsilon}_h(\mathbf{v}_h)), \\ \boldsymbol{\sigma}_h(\mathbf{v}_h) &:= \frac{E}{1+\nu} \left(\boldsymbol{\epsilon}_h(\mathbf{v}_h) + \frac{\nu}{1-2\nu} \operatorname{div}_h(\mathbf{v}_h) \mathbf{I}_3 \right). \end{aligned} \quad (3.4)$$

The scheme for the contact mechanics problem reads: Find $(\mathbf{u}_h, \boldsymbol{\lambda}_h) \in \mathbf{X}_{\mathbf{grad},h,0} \times \mathcal{C}_{f,h}$ such that, for all $(\mathbf{v}_h, \boldsymbol{\mu}_h) \in \mathbf{X}_{\mathbf{grad},h,0} \times \mathcal{C}_{f,h}$,

$$\int_\Omega \boldsymbol{\sigma}_h(\mathbf{u}_h) : \boldsymbol{\epsilon}_h(\mathbf{v}_h) + \mu_1 \mathbb{S}_h(\mathbf{u}_h, \mathbf{v}_h) + \int_\Gamma \boldsymbol{\lambda}_h \cdot [[\mathbf{v}_h]]_h = \sum_{K \in \mathcal{M}} \int_K \mathbf{f} \cdot \mathbf{v}_K, \quad (3.5a)$$

$$\int_{\Gamma} (\boldsymbol{\mu}_h - \boldsymbol{\lambda}_h) \cdot \llbracket \underline{\mathbf{u}}_h \rrbracket_h \leq 0. \quad (3.5b)$$

Here \mathbb{S}_h is the stabilisation bilinear form defined by

$$\mathbb{S}_h(\underline{\mathbf{u}}_h, \underline{\mathbf{v}}_h) := \sum_{K \in \mathcal{M}} \mathbb{S}_K(\underline{\mathbf{u}}_h, \underline{\mathbf{v}}_h)$$

with local stabilisation bilinear forms $\mathbb{S}_K : \mathbb{X}_{\mathbf{grad},h}^1 \times \mathbb{X}_{\mathbf{grad},h}^1 \rightarrow \mathbb{R}$ given by

$$\begin{aligned} \mathbb{S}_K(\underline{\mathbf{u}}_h, \underline{\mathbf{v}}_h) &= h_K^{-1} \sum_{\sigma \in \mathcal{F}_K} \int_{\sigma} (\Upsilon_K^2 \underline{\mathbf{u}}_h - \Upsilon_{K\sigma}^2 \underline{\mathbf{u}}_h) \cdot (\Upsilon_K^2 \underline{\mathbf{v}}_h - \Upsilon_{K\sigma}^2 \underline{\mathbf{v}}_h) \\ &\quad + \sum_{e \in \mathcal{E}_K} \int_e (\Upsilon_K^2 \underline{\mathbf{u}}_h - \Upsilon_{Ke}^2 \underline{\mathbf{u}}_h) \cdot (\Upsilon_K^2 \underline{\mathbf{v}}_h - \Upsilon_{Ke}^2 \underline{\mathbf{v}}_h) \\ &\quad + h_K \sum_{s \in \mathcal{V}_K} (\Upsilon_K^2 \underline{\mathbf{u}}_h(\mathbf{x}_s) - \mathbf{u}_{Ks}) \cdot (\Upsilon_K^2 \underline{\mathbf{v}}_h(\mathbf{x}_s) - \mathbf{v}_{Ks}). \end{aligned} \quad (3.6)$$

Next we define the broken H^1 -like semi-norm on $\mathbf{X}_{\mathbf{grad},h}$ as: for all $\underline{\mathbf{v}}_h \in \mathbf{X}_{\mathbf{grad},h}$:

$$\|\underline{\mathbf{v}}_h\|_{1,h} := \left(\sum_{K \in \mathcal{M}} \|\underline{\mathbf{v}}_h\|_{1,K}^2 \right)^{1/2} \quad \text{with} \quad \|\underline{\mathbf{v}}_h\|_{1,K}^2 := \|\mathbb{G}_K^1 \underline{\mathbf{v}}_h\|_{L^2(K)}^2 + \mathbb{S}_K(\underline{\mathbf{v}}_h, \underline{\mathbf{v}}_h). \quad (3.7)$$

Note that, through the terms \mathbb{S}_K , this norm bounds the jump between each element components and its faces/edges/vertices components. Due to the single-valuedness of components on faces/edges/vertices that are not on the fracture network, this norm therefore bounds inter-element jumps that do not occur across the fracture network.

Theorem 3.1 (Discrete Korn Inequality). *It holds*

$$\|\underline{\mathbf{v}}_h\|_{1,h}^2 \lesssim \|\boldsymbol{\epsilon}_h(\underline{\mathbf{v}}_h)\|_{L^2(\Omega \setminus \bar{\Gamma})}^2 + \mathbb{S}_h(\underline{\mathbf{v}}_h, \underline{\mathbf{v}}_h) \quad \forall \underline{\mathbf{v}}_h \in \mathbf{X}_{\mathbf{grad},h,0}. \quad (3.8)$$

Proof. See Section 5.1. □

For notational convenience, let us define the discrete energy inner product $\langle \cdot, \cdot \rangle_{\text{en},h}$ such that, for all $\underline{\mathbf{v}}_h, \underline{\mathbf{w}}_h \in \mathbf{X}_{\mathbf{grad},h,0}$,

$$\langle \underline{\mathbf{v}}_h, \underline{\mathbf{w}}_h \rangle_{\text{en},h} := \int_{\Omega} \boldsymbol{\sigma}_h(\underline{\mathbf{v}}_h) : \boldsymbol{\epsilon}_h(\underline{\mathbf{w}}_h) + \mu_1 \mathbb{S}_h(\underline{\mathbf{v}}_h, \underline{\mathbf{w}}_h), \quad (3.9)$$

where $\mathbb{S}_h = \sum_{K \in \mathcal{M}} \mathbb{S}_K(\underline{\mathbf{u}}_h, \underline{\mathbf{v}}_h)$ and μ_1 is, as in Section 2, a lower bound of $E/(1+\nu)$. This bilinear form is indeed an inner product by the discrete Korn inequality (3.8), $\mu_1 \leq \frac{E}{1+\nu}$, and the definition (3.4) of $\boldsymbol{\sigma}_h$, which shows that

$$\mu_1 \|\underline{\mathbf{v}}_h\|_{1,h}^2 \leq \tilde{C} \|\underline{\mathbf{v}}_h\|_{\text{en},h}^2, \quad (3.10)$$

where $\|\cdot\|_{\text{en},h}$ is the norm induced by the inner product $\langle \cdot, \cdot \rangle_{\text{en},h}$ and the constant \tilde{C} is independent of E and ν .

Definition 3.1 ($H^{-1/2}$ -like norm on $L^2(\Gamma)^3$). The norm $\|\cdot\|_{-1/2,\Gamma}$ on $L^2(\Gamma)^3$ is defined by: for all $\boldsymbol{\lambda} \in L^2(\Gamma)^3$,

$$\|\boldsymbol{\lambda}\|_{-1/2,\Gamma} := \sup_{\mathbf{v} \in H_0^1(\Omega \setminus \Gamma)^3 \setminus \{0\}} \frac{\int_{\Gamma} \boldsymbol{\lambda} \cdot \llbracket \mathbf{v} \rrbracket}{\|\mathbf{v}\|_{H^1(\Omega \setminus \Gamma)}}. \quad (3.11)$$

Remark 3.1 (Comparison with the norm in [32]). This discrete $H^{-1/2}$ -like norm is simpler than that in [32, Definition 4.3], which is made possible by our use of a higher-order scheme for the displacement that involves face degrees of freedom on both sides of the fracture.

Theorem 3.2 (Discrete inf-sup condition). *It holds*

$$\sup_{\mathbf{v}_h \in \mathbf{X}_{\text{grad},h,0} \setminus \{0\}} \frac{\int_{\Gamma} \boldsymbol{\lambda}_h \cdot \llbracket \mathbf{v}_h \rrbracket_h}{\|\mathbf{v}_h\|_{1,h}} \gtrsim \|\boldsymbol{\lambda}_h\|_{-1/2,\Gamma} \quad \forall \boldsymbol{\lambda}_h \in \mathbf{M}_h. \quad (3.12)$$

Proof. See Section 5.2. □

Proposition 3.3 (Existence and uniqueness result). *There exists a unique solution $(\underline{\mathbf{u}}_h, \boldsymbol{\lambda}_h) \in \mathbf{X}_{\text{grad},h,0} \times \mathcal{C}_{f,h}$ to (3.5).*

Proof. The abstract framework of [39, Theorem 3.8] on saddle point problems gives the existence of a solution. The uniqueness of $\underline{\mathbf{u}}_h$ derives from the discrete Korn inequality (3.8) and the uniqueness of $\boldsymbol{\lambda}_h$ from the discrete inf-sup property (3.12), as demonstrated in [32, Proposition 4.1]. □

4 Main results

We denote by $C_0^0(\bar{\Omega} \setminus \Gamma)$ the set of continuous functions $\bar{\Omega} \setminus \Gamma \rightarrow \mathbb{R}$ that vanish on $\partial\Omega$. The interpolator $\mathbb{I}_h : C_0^0(\bar{\Omega} \setminus \Gamma)^3 \rightarrow \mathbf{X}_{\text{grad},h}$ is defined as follows: for all $\mathbf{v} \in C_0^0(\bar{\Omega} \setminus \Gamma)^3$,

$$\mathbb{I}_h \mathbf{v} := \left((\mathbb{I}_{\mathcal{K}s} \mathbf{v})_{K \in \mathcal{M}}, s \in \mathcal{V}_K, (\mathbb{I}_{\mathcal{K}e} \mathbf{v})_{K \in \mathcal{M}}, e \in \mathcal{E}_K, (\mathbb{I}_{\mathcal{K}\sigma} \mathbf{v})_{K \in \mathcal{M}}, \sigma \in \mathcal{F}_K, (\mathbb{I}_K \mathbf{v})_{K \in \mathcal{M}} \right),$$

where

$$\begin{aligned} \mathbb{I}_{\mathcal{K}s} \mathbf{v} &= \mathbf{v}|_K(\mathbf{x}_s) & \forall s \in \mathcal{V}_K, K \in \mathcal{M}, \\ \mathbb{I}_{\mathcal{K}e} \mathbf{v} &= \Pi_e^0(\mathbf{v}|_K) & \forall e \in \mathcal{E}_K, K \in \mathcal{M}, \\ \mathbb{I}_{\mathcal{K}\sigma} \mathbf{v} &= \Pi_\sigma^0(\mathbf{v}|_K) & \forall \sigma \in \mathcal{F}_K, K \in \mathcal{M}, \end{aligned} \quad (4.1a)$$

$$\mathbb{I}_K \mathbf{v} = \Pi_K^0 \mathbf{v} + \tilde{\mathbf{v}}_K \quad \forall K \in \mathcal{M}, \quad (4.1b)$$

and $\tilde{\mathbf{v}}_K \in \mathbb{R}^3$ is defined by

$$\int_K \tilde{\mathbf{v}}_K \cdot \nabla \phi = - \sum_{\sigma \in \mathcal{F}_K} \int_{\sigma} (\mathbf{v}|_K - \Upsilon_{\mathcal{K}\sigma}^2 \mathbb{I}_h \mathbf{v}) \cdot \phi \mathbf{n}_{\mathcal{K}\sigma} \quad \forall \phi \in \mathbb{P}^1(K). \quad (4.2)$$

Remark 4.1 (Definition of the interpolator). We note that the definition (4.2) is not self-referencing (and therefore makes sense): even though the interpolate $\mathbb{I}_h \mathbf{v}$ appears in the right-hand side, this is through the reconstruction $\Upsilon_{\mathcal{K}\sigma}^2$ which only relies on the – already defined – values of the interpolate on vertices, edges, and faces, not on K (for which $\tilde{\mathbf{v}}_K$ must be defined). Moreover, (4.2) properly fixes a unique vector in \mathbb{R}^3 because $\nabla : P^1(K)/\mathbb{R} \rightarrow \mathbb{R}^3$ is an isomorphism and, if ϕ is constant, the right-hand side vanishes by (4.3) below.

In the definition (4.1b) of the cell component of $\mathbb{I}_h \mathbf{v}$, the correction $\tilde{\mathbf{v}}_K$ to the L^2 -projection $\Pi_K^0(\mathbf{v}|_K)$ is required to ensure that \mathbb{I}_h is a Fortin interpolator for the divergence, see Lemma 5.5. We note however that, if $\mathbf{v} \in \mathbb{P}^2(K)^3$, then $\Upsilon_{\mathcal{K}\sigma}^2 \mathbb{I}_h \mathbf{v} = (\mathbf{v}|_K)|_\sigma$, so $\tilde{\mathbf{v}}_K = 0$. This correction is therefore a higher-than-quadratic correction to the interpolator.

Lemma 4.1 (Properties of the reconstruction operators). *The edge, face, and element gradients, and reconstruction operators satisfy the following properties:*

$$\Pi_\sigma^0 \Upsilon_{K\sigma}^2(\mathbf{v}_h) = \mathbf{v}_{K\sigma} \quad \forall \sigma \in \mathcal{F}, \forall \mathbf{v}_h \in \mathbf{X}_{\mathbf{grad},h}, \quad (4.3)$$

$$\Pi_K^0 \Upsilon_K^2(\mathbf{v}_h) = \mathbf{v}_K \quad \forall K \in \mathcal{M}, \forall \mathbf{v}_h \in \mathbf{X}_{\mathbf{grad},h}, \quad (4.4)$$

$$\mathbb{G}_K^1 \mathbb{I}_h \mathbf{q} = \nabla \mathbf{q} \quad \forall K \in \mathcal{M}, \forall \mathbf{q} \in \mathbb{P}^2(K)^3, \quad (4.5)$$

$$\Upsilon_K^2 \mathbb{I}_h \mathbf{q} = \mathbf{q} \quad \forall K \in \mathcal{M}, \forall \mathbf{q} \in \mathbb{P}^2(K)^3, \quad (4.6)$$

$$\Upsilon_{Ke}^2 \mathbb{I}_h \mathbf{q} = \mathbf{q} \quad \forall K \in \mathcal{M}, \forall e \in \mathcal{E}_K, \forall \mathbf{q} \in \mathbb{P}^2(e)^3, \quad (4.7)$$

$$\Upsilon_{K\sigma}^2 \mathbb{I}_h \mathbf{q} = \mathbf{q} \quad \forall K \in \mathcal{M}, \forall \sigma \in \mathcal{F}_K, \forall \mathbf{q} \in \mathbb{P}^2(\sigma)^3,$$

where, by abuse of notation, the interpolator \mathbb{I}_h applied to functions only defined on a mesh entity (cell, face, or edge) corresponds to the restriction of the degrees of freedom (4.1) belonging to that mesh entity (notice that the gradient or displacement reconstructions on the corresponding mesh entity only depend on these degrees of freedom).

Proof. We refer to [26, Lemma 3] for the proof of this lemma, using Remark 4.1 for (4.5) and (4.6). \square

Following the approach of the Gradient Discretisation Method [28], the abstract error estimate will be stated in terms of two quantities measuring the (primal) consistency and the limit-conformity (also known as adjoint consistency) of the discrete space and operators.

- The primal consistency error is: for $\mathbf{v}_h \in \mathbf{X}_{\mathbf{grad},h,0}$,

$$\mathfrak{C}_h(\mathbf{u}, \mathbf{v}_h) := \left(\|\nabla \mathbf{u} - \mathbb{G}_h^1 \mathbf{v}_h\|_{L^2(\Omega \setminus \bar{\Gamma})}^2 + \mathbb{S}_h(\mathbf{v}_h, \mathbf{v}_h) \right)^{1/2}. \quad (4.8)$$

- Letting

$$\Sigma := \{\boldsymbol{\chi} \in H_{\text{div}}(\Omega \setminus \bar{\Gamma}; \mathcal{S}^3(\mathbb{R})), : \gamma_{\mathbf{n}}^+ \boldsymbol{\chi} + \gamma_{\mathbf{n}}^- \boldsymbol{\chi} = \mathbf{0}, \gamma_{\mathbf{n}}^+ \boldsymbol{\chi} \in L^2(\Gamma)\},$$

(where $\mathcal{S}^3(\mathbb{R})$ is the space of symmetric 3×3 matrices with real coefficients), the limit-conformity measure is defined as, for $\boldsymbol{\chi} \in \Sigma$:

$$\mathcal{W}_h(\boldsymbol{\chi}) := \sup_{\mathbf{v}_h \in \mathbf{X}_{\mathbf{grad},h,0}} \frac{w_h(\boldsymbol{\chi}, \mathbf{v}_h)}{\|\mathbf{v}_h\|_{1,h}}, \quad (4.9)$$

where $w_h(\boldsymbol{\chi}, \mathbf{v}_h) := - \int_{\Omega} \boldsymbol{\chi} : \boldsymbol{\epsilon}_h(\mathbf{v}_h) + \int_{\Gamma} \Pi_{\mathcal{F}_\Gamma}^0(\gamma_{\mathbf{n}}^+ \boldsymbol{\chi}) \cdot \llbracket \mathbf{v}_h \rrbracket_h - \sum_{K \in \mathcal{M}} \int_K \mathbf{v}_K \cdot \text{div } \boldsymbol{\chi}$.

The term ‘‘adjoint consistency’’ refers to the fact that $\mathcal{W}_h(\boldsymbol{\chi})$ measures a defect of integration-by-parts formula between the discrete strain and the continuous divergence; put another way, it measures how well some formal adjoint of the discrete strain approximates the divergence.

Theorem 4.2 (Abstract error estimate). *Let $(\mathbf{u}, \boldsymbol{\lambda})$ be the solution to (2.2) and assume that $\mathbf{u} \in H_0^1(\Omega \setminus \bar{\Gamma})^3 \cap H^{\frac{3}{2}+\mathfrak{r}}(\mathcal{M})^3$ for some $0 < \mathfrak{r} \leq 1$. Then, the solution $(\mathbf{u}_h, \boldsymbol{\lambda}_h)$ of (3.5) satisfies the following error estimate:*

$$\|\mathbb{I}_h \mathbf{u} - \mathbf{u}_h\|_{\text{en},h} \lesssim \frac{1}{\sqrt{\mu_1}} \mathcal{W}_h(\boldsymbol{\sigma}(\mathbf{u})) + \sqrt{\mu_2} \mathfrak{C}_h(\mathbf{u}, \mathbb{I}_h \mathbf{u})$$

$$+ \max \left[0; \int_{\Gamma} (\boldsymbol{\lambda} - \Pi_{\mathcal{F}_\Gamma}^0 \boldsymbol{\lambda}) \cdot (\llbracket \mathbf{u} \rrbracket - \Pi_{\mathcal{F}_\Gamma}^0 \llbracket \mathbf{u} \rrbracket) \right]^{1/2}, \quad (4.10)$$

$$\begin{aligned} \|\boldsymbol{\lambda} - \boldsymbol{\lambda}_h\|_{-1/2, \Gamma} &\lesssim \mathcal{W}_h(\boldsymbol{\sigma}(\mathbf{u})) + \mu_2 \boldsymbol{\mathfrak{E}}_h(\mathbf{u}, \mathbb{I}_h \mathbf{u}) + \|\boldsymbol{\lambda} - \Pi_{\mathcal{F}_\Gamma}^0 \boldsymbol{\lambda}\|_{-1/2, \Gamma} \\ &\quad + \sqrt{\mu_2} \left(1 + \left(\frac{\nu}{1-2\nu} \right)^{\frac{1}{2}} \right) \|\underline{\mathbf{u}}_h - \mathbb{I}_h \mathbf{u}\|_{\text{en}, h}. \end{aligned} \quad (4.11)$$

Remark 4.2 (Locking-free estimate). Recalling that the hidden multiplicative constant in \lesssim does not depend on the Poisson ratio, we notice that the error bound (4.10) on the matrix displacement does not contain any constant that blows up in the incompressible limit $\nu \rightarrow \frac{1}{2}$, whereas the term $\frac{1}{\sqrt{1-2\nu}}$ in the right-hand side of the estimate (4.11) on the Lagrange multiplier does blow up in this limit; this is not unexpected since this Lagrange multiplier plays the role of a traction, whose definition explicitly involve such a term.

Theorem 4.3 (Error estimate). *Let $(\mathbf{u}, \boldsymbol{\lambda})$ be the solution to (2.2). Consider real parameters \mathfrak{r} and $s_\mathfrak{r}$ satisfying*

- If $g = 0$ (no friction): $0 \leq \mathfrak{r} < 1$, $s_\mathfrak{r} = \mathfrak{r}$, and $t_\mathfrak{r} = 1 + \mathfrak{r}$.
- If $g \neq 0$ (friction): $0 \leq \mathfrak{r} \leq 1/2$, $s_\mathfrak{r} = 2\mathfrak{r}$, and $t_\mathfrak{r} = 1$.

Assume that $\mathbf{u} \in H_0^1(\Omega \setminus \bar{\Gamma})^3 \cap H^{\frac{3}{2}+\mathfrak{r}}(\mathcal{M})^3$ and $\boldsymbol{\lambda} \in H^{s_\mathfrak{r}}(\Gamma)^3$. Then, the discrete solution $(\underline{\mathbf{u}}_h, \boldsymbol{\lambda}_h)$ of (3.5) satisfies the following error estimates:

$$\begin{aligned} \|\underline{\mathbf{u}}_h - \mathbb{I}_h \mathbf{u}\|_{\text{en}, h} &\lesssim h^{\frac{1}{2}+\mathfrak{r}} \left[\frac{1}{\sqrt{\mu_1}} \left(|\boldsymbol{\sigma}(\mathbf{u})|_{H^{\frac{1}{2}+\mathfrak{r}}(\mathcal{M})} + |\boldsymbol{\lambda}|_{H^\mathfrak{r}(\Gamma)} \right) + \sqrt{\mu_2} |\mathbf{u}|_{H^{\frac{3}{2}+\mathfrak{r}}(\mathcal{M})} \right. \\ &\quad \left. + |\boldsymbol{\lambda}|_{H^{s_\mathfrak{r}}(\Gamma)} + \|\llbracket \mathbf{u} \rrbracket\|_{H^{t_\mathfrak{r}}(\Gamma)} \right], \end{aligned} \quad (4.12)$$

$$\begin{aligned} \|\boldsymbol{\lambda} - \boldsymbol{\lambda}_h\|_{-1/2, \Gamma} &\lesssim h^{\frac{1}{2}+\mathfrak{r}} \left(|\boldsymbol{\sigma}(\mathbf{u})|_{H^{\frac{1}{2}+\mathfrak{r}}(\mathcal{M})} + \mu_2 |\mathbf{u}|_{H^{\frac{3}{2}+\mathfrak{r}}(\mathcal{M})} + |\boldsymbol{\lambda}|_{H^\mathfrak{r}(\Gamma)} \right) \\ &\quad + \sqrt{\mu_2} \left(1 + \left(\frac{\nu}{1-2\nu} \right)^{\frac{1}{2}} \right) \|\underline{\mathbf{u}}_h - \mathbb{I}_h \mathbf{u}\|_{\text{en}, h}, \end{aligned} \quad (4.13)$$

where we recall that the hidden constants in \lesssim do not depend on the Young modulus E or the Poisson ratio ν .

Remark 4.3 (Error estimates). The error estimate (4.12) is (potentially, if the solution is smooth enough) better in the case of no-friction, since \mathfrak{r} is then allowed to go almost to 1, instead of being limited to 1/2 in case of friction. We note that the contact mechanics problem is presented for quadratic finite elements in [45] but that the analysis in this reference, which allows for $0 \leq \mathfrak{r} < 1$, is only performed in the case of zero Tresca threshold g . It is unclear at the moment if the analysis allowing for larger \mathfrak{r} can be adapted (in the case of finite elements or our scheme) to the case $g \neq 0$. Our numerical simulations however indicate that the higher accuracy is also achieved in the latter case.

5 Proof of error estimates

We start this section with bounds involving face operators.

Lemma 5.1. For all $\underline{\mathbf{v}}_h \in \mathbf{X}_{\text{grad},h}$ and $K \in \mathcal{M}$, the following relations hold:

$$\|\underline{\mathbf{v}}_h\|_{1,K}^2 \approx \|\nabla \Upsilon_K^2 \underline{\mathbf{v}}_h\|_{L^2(K)}^2 + \mathbb{S}_K(\underline{\mathbf{v}}_h, \underline{\mathbf{v}}_h), \quad (5.1)$$

$$h_K \|\nabla_\sigma \Upsilon_{K\sigma}^2 \underline{\mathbf{v}}_h\|_{L^2(\sigma)}^2 \lesssim \|\underline{\mathbf{v}}_h\|_{1,K}^2 \quad \forall \sigma \in \mathcal{F}_K, \quad (5.2)$$

$$h_K^{-1} \|\mathbf{v}_K - \Upsilon_{K\sigma}^2 \underline{\mathbf{v}}_h\|_{L^2(\sigma)}^2 \lesssim \|\underline{\mathbf{v}}_h\|_{1,K}^2 \quad \forall \sigma \in \mathcal{F}_K, \quad (5.3)$$

where ∇_σ is the tangential gradient on σ .

Proof. Let $\underline{\mathbf{v}}_h \in \mathbf{X}_{\text{grad},h}$ and $K \in \mathcal{M}$. For every $\boldsymbol{\xi} \in \mathbb{P}^1(K)^{3 \times 3}$, we have

$$\begin{aligned} \int_K \nabla \Upsilon_K^2 \underline{\mathbf{v}}_h : \boldsymbol{\xi} &\stackrel{\text{IBP}, (4.4)}{=} - \int_K \mathbf{v}_K \cdot \text{div}(\boldsymbol{\xi}) + \sum_{\sigma \in \mathcal{F}_K} \int_\sigma \Upsilon_K^2 \underline{\mathbf{v}}_h \cdot \boldsymbol{\xi} \mathbf{n}_{K\sigma} \\ &\stackrel{(3.3)}{=} \int_K \mathbb{G}_K^1 \underline{\mathbf{v}}_h : \boldsymbol{\xi} + \sum_{\sigma \in \mathcal{F}_K} \int_\sigma (\Upsilon_K^2 \underline{\mathbf{v}}_h - \Upsilon_{K\sigma}^2 \underline{\mathbf{v}}_h) \cdot \boldsymbol{\xi} \mathbf{n}_{K\sigma} \\ &\leq \int_K \mathbb{G}_K^1 \underline{\mathbf{v}}_h : \boldsymbol{\xi} + \sum_{\sigma \in \mathcal{F}_K} \|\Upsilon_K^2 \underline{\mathbf{v}}_h - \Upsilon_{K\sigma}^2 \underline{\mathbf{v}}_h\|_{L^2(\sigma)} \|\boldsymbol{\xi}\|_{L^2(\sigma)}. \end{aligned}$$

Applying the discrete trace inequality [25, Lemma 1.32] to $\boldsymbol{\xi}$, we infer

$$\int_K (\nabla \Upsilon_K^2 \underline{\mathbf{v}}_h - \mathbb{G}_K^1 \underline{\mathbf{v}}_h) : \boldsymbol{\xi} \lesssim \left(\sum_{\sigma \in \mathcal{F}_K} h_K^{-1/2} \|\Upsilon_K^2 \underline{\mathbf{v}}_h - \Upsilon_{K\sigma}^2 \underline{\mathbf{v}}_h\|_{L^2(\sigma)} \right) \|\boldsymbol{\xi}\|_{L^2(K)}. \quad (5.4)$$

Taking $\boldsymbol{\xi} = \nabla \Upsilon_K^2 \underline{\mathbf{v}}_h - \mathbb{G}_K^1 \underline{\mathbf{v}}_h \in \mathbb{P}^1(K)^{3 \times 3}$ and simplifying, we obtain

$$\|\nabla \Upsilon_K^2 \underline{\mathbf{v}}_h - \mathbb{G}_K^1 \underline{\mathbf{v}}_h\|_{L^2(K)} \lesssim \sum_{\sigma \in \mathcal{F}_K} h_K^{-1/2} \|\Upsilon_K^2 \underline{\mathbf{v}}_h - \Upsilon_{K\sigma}^2 \underline{\mathbf{v}}_h\|_{L^2(\sigma)} \stackrel{(3.6)}{\leq} \mathbb{S}_K(\underline{\mathbf{v}}_h, \underline{\mathbf{v}}_h)^{1/2}. \quad (5.5)$$

The norm equivalence (5.1) follows by combining triangles inequalities, the definition (3.7) of $\|\cdot\|_{1,K}$, and (5.5).

Next, assume that $\sigma \in \mathcal{F}_K$ is a generic face of K . The relation (5.2) follows by using the triangle inequality, the bound $|\nabla_\sigma \Upsilon_{K\sigma}^2 \underline{\mathbf{v}}_h| \leq |\nabla \Upsilon_K^2 \underline{\mathbf{v}}_h|$, the discrete inverse and trace inequalities [25, Lemmas 1.28 and 1.32], the relation $h_K \approx h_\sigma$ (resulting from the mesh regularity assumption) and (3.6) to write

$$\begin{aligned} \|\nabla_\sigma \Upsilon_{K\sigma}^2 \underline{\mathbf{v}}_h\|_{L^2(\sigma)}^2 &\lesssim \|\nabla_\sigma (\Upsilon_{K\sigma}^2 \underline{\mathbf{v}}_h - \Upsilon_K^2 \underline{\mathbf{v}}_h)\|_{L^2(\sigma)}^2 + \|\nabla \Upsilon_K^2 \underline{\mathbf{v}}_h\|_{L^2(\sigma)}^2 \\ &\lesssim h_K^{-2} \|\Upsilon_{K\sigma}^2 \underline{\mathbf{v}}_h - \Upsilon_K^2 \underline{\mathbf{v}}_h\|_{L^2(\sigma)}^2 + h_K^{-1} \|\nabla \Upsilon_K^2 \underline{\mathbf{v}}_h\|_{L^2(K)}^2 \\ &\stackrel{(3.6)}{\lesssim} h_K^{-1} \left(\mathbb{S}_K(\underline{\mathbf{v}}_h, \underline{\mathbf{v}}_h) + \|\nabla \Upsilon_K^2 \underline{\mathbf{v}}_h\|_{L^2(K)}^2 \right) \\ &\stackrel{(5.1)}{\approx} h_K^{-1} \|\underline{\mathbf{v}}_h\|_{1,K}^2. \end{aligned}$$

Furthermore, using (4.4), the triangle inequality, the discrete trace inequality [25, Lemma 1.32] and the approximation properties of Π_K^0 [25, Theorem 1.45], we obtain

$$\begin{aligned} \|\mathbf{v}_K - \Upsilon_{K\sigma}^2 \underline{\mathbf{v}}_h\|_{L^2(\sigma)} &\leq \|\Pi_K^0 \Upsilon_K^2 \underline{\mathbf{v}}_h - \Upsilon_K^2 \underline{\mathbf{v}}_h\|_{L^2(\sigma)} + \|\Upsilon_K^2 \underline{\mathbf{v}}_h - \Upsilon_{K\sigma}^2 \underline{\mathbf{v}}_h\|_{L^2(\sigma)} \\ &\stackrel{(3.6)}{\lesssim} h_K^{-1/2} \|\Pi_K^0 \Upsilon_K^2 \underline{\mathbf{v}}_h - \Upsilon_K^2 \underline{\mathbf{v}}_h\|_{L^2(K)} + h_K^{1/2} \mathbb{S}_K(\underline{\mathbf{v}}_h, \underline{\mathbf{v}}_h)^{1/2} \end{aligned}$$

$$\begin{aligned}
&\lesssim h_K^{1/2} \left(\|\nabla \Upsilon_K^2 \underline{\mathbf{v}}_h\|_K + \mathbb{S}_K(\underline{\mathbf{v}}_h, \underline{\mathbf{v}}_h)^{1/2} \right) \\
&\stackrel{(5.1)}{\approx} h_K^{1/2} \|\underline{\mathbf{v}}_h\|_{1,K}. \quad \square
\end{aligned}$$

The following lemma provides a DOF-based bound on the discrete norm, which plays a crucial role in proving the bound on the consistency of the gradient reconstruction (Lemma 5.8).

Lemma 5.2. *Let $K \in \mathcal{M}$ and $\underline{\mathbf{v}}_h \in \mathbf{X}_{\text{grad},h}$. Then, it holds:*

$$\|\underline{\mathbf{v}}_h\|_{1,K} \lesssim h_K^{1/2} \left(|\mathbf{v}_K| + \max_{\sigma \in \mathcal{F}_K} |\mathbf{v}_{K\sigma}| + \max_{e \in \mathcal{E}_K} |\mathbf{v}_{Ke}| + \max_{s \in \mathcal{V}_K} |\mathbf{v}_{Ks}| \right). \quad (5.6)$$

Proof. Recalling the definition (3.7) of $\|\cdot\|_{1,K}$, we will begin by finding a bound on $\mathbb{S}_K(\underline{\mathbf{v}}_h, \underline{\mathbf{v}}_h)$. To this purpose, we use triangle and discrete trace inequalities [25, Lemma 1.32] to write

$$\begin{aligned}
\mathbb{S}_K(\underline{\mathbf{v}}_h, \underline{\mathbf{v}}_h) &= h_K^{-1} \sum_{\sigma \in \mathcal{F}_K} \|\Upsilon_K^2 \underline{\mathbf{v}}_h - \Upsilon_{K\sigma}^2 \underline{\mathbf{v}}_h\|_{L^2(\sigma)}^2 + \sum_{e \in \mathcal{E}_K} \|\Upsilon_K^2 \underline{\mathbf{v}}_h - \Upsilon_{Ke}^2 \underline{\mathbf{v}}_h\|_{L^2(e)}^2 \\
&\quad + h_K \sum_{s \in \mathcal{V}_K} |\Upsilon_K^2 \underline{\mathbf{v}}_h(\mathbf{x}_s) - \mathbf{v}_{Ks}|^2 \\
&\lesssim h_K^{-2} \|\Upsilon_K^2 \underline{\mathbf{v}}_h\|_{L^2(K)}^2 + \max_{\sigma \in \mathcal{F}_K} h_K^{-1} \|\Upsilon_{K\sigma}^2 \underline{\mathbf{v}}_h\|_{L^2(\sigma)}^2 + \max_{e \in \mathcal{E}_K} \|\Upsilon_{Ke}^2 \underline{\mathbf{v}}_h\|_{L^2(e)}^2 + h_K \max_{s \in \mathcal{V}_K} |\mathbf{v}_{Ks}|^2.
\end{aligned}$$

Now, the estimates of [21, Lemma 8] give

$$\begin{aligned}
\|\Upsilon_{Ke}^2 \underline{\mathbf{v}}_h\|_{L^2(e)} &\lesssim \|\mathbf{v}_{Ke}\|_{L^2(e)} + h_e^{1/2} \sum_{s \in \mathcal{V}_e} |\mathbf{v}_{Ks}|, \\
\|\Upsilon_{K\sigma}^2 \underline{\mathbf{v}}_h\|_{L^2(\sigma)} &\lesssim \|\mathbf{v}_{K\sigma}\|_{L^2(\sigma)} + h_\sigma^{1/2} \sum_{e \in \mathcal{E}_\sigma} \|\Upsilon_{Ke}^2 \underline{\mathbf{v}}_h\|_{L^2(e)} + h_\sigma \sum_{s \in \mathcal{V}_\sigma} |\mathbf{v}_{Ks}|, \\
\|\Upsilon_K^2 \underline{\mathbf{v}}_h\|_{L^2(K)} &\lesssim \|\mathbf{v}_K\|_{L^2(K)} + h_K^{1/2} \sum_{\sigma \in \mathcal{F}_K} \|\mathbf{v}_{K\sigma}\|_{L^2(\sigma)} + h_K \sum_{e \in \mathcal{E}_K} \|\Upsilon_{Ke}^2 \underline{\mathbf{v}}_h\|_{L^2(e)} + h_K^{3/2} \sum_{s \in \mathcal{V}_K} |\mathbf{v}_{Ks}|. \quad (5.7)
\end{aligned}$$

Using triangle inequality, equation (5.1), and mesh regularity (which gives $h_e \approx h_\sigma \approx h_K$), we obtain

$$\mathbb{S}_K(\underline{\mathbf{v}}_h, \underline{\mathbf{v}}_h) \lesssim h_K^{-2} \|\mathbf{v}_K\|_{L^2(K)}^2 + \max_{\sigma \in \mathcal{F}_K} h_K^{-1} \|\mathbf{v}_{K\sigma}\|_{L^2(\sigma)}^2 + \max_{e \in \mathcal{E}_K} \|\mathbf{v}_{Ke}\|_{L^2(e)}^2 + h_K \max_{s \in \mathcal{V}_K} |\mathbf{v}_{Ks}|^2.$$

Since, all of $\mathbf{v}_K, \mathbf{v}_{K\sigma}, \mathbf{v}_{Ke}$, and \mathbf{v}_{Ks} are constant, a use of mesh regularity (which gives $|e| \approx h_K$, $|\sigma| \approx h_K^2$ and $|K| \approx h_K^3$) shows that $\mathbb{S}_K(\underline{\mathbf{v}}_h, \underline{\mathbf{v}}_h)^{1/2}$ is bounded above by the right-hand side of (5.6). The bound on $\|\underline{\mathbf{v}}_h\|_{1,K}$ then follows from (5.1), the bound (5.7), and an inverse inequality. \square

5.1 Proof of the discrete Korn Inequality (Theorem 3.1)

Recalling (5.1), to prove the inequality (3.8), we just need to bound $\|\nabla_{\mathcal{M}} \Upsilon_h^2 \underline{\mathbf{v}}_h\|_{L^2(\Omega \setminus \bar{\Gamma})}$ (where $\nabla_{\mathcal{M}}$ is the broken gradient on \mathcal{M}). Applying the same techniques as in [32, Theorem 5.7] (which consist in adapting the node-averaging approach of [25, Section 7.3.2] to the case of a fractured medium), we obtain

$$\|\nabla_{\mathcal{M}} \Upsilon_h^2 \underline{\mathbf{v}}_h\|_{L^2(\Omega)}^2 \lesssim \|\epsilon_{\mathcal{M}}(\Upsilon_h^2 \underline{\mathbf{v}}_h)\|_{L^2(\Omega \setminus \bar{\Gamma})}^2 + \sum_{\sigma \in \mathcal{F} \setminus \mathcal{F}_\Gamma} h_\sigma^{-1} \|[\Upsilon_h^2 \underline{\mathbf{v}}_h]\|_{L^2(\sigma)}^2, \quad (5.8)$$

where $\epsilon_{\mathcal{M}}$ is the broken strain on \mathcal{M} and, for all $\sigma = K|L \in \mathcal{F}^{\text{int}}$, $|\llbracket \Upsilon_h^2 \mathbf{v}_h \rrbracket|_{\sigma} = |\Upsilon_K^2 \mathbf{v}_h - \Upsilon_L^2 \mathbf{v}_h|$ while, if $\sigma \in \mathcal{F}^{\text{ext}} \cap \mathcal{F}_K$, $|\llbracket \Upsilon_h^2 \mathbf{v}_h \rrbracket|_{\sigma} = |\Upsilon_K^2 \mathbf{v}_h|$. Note that, in (5.8), thanks to the modified node-averaging operator of [32, Theorem 5.7] only jumps across non-fracture faces appear; this will be essential below as only these jumps can be bounded above using the stabilisation \mathbb{S}_h .

Recalling (5.4), taking $\boldsymbol{\xi} = \epsilon_{\mathcal{M}}(\Upsilon_h^2 \mathbf{v}_h)|_K - \epsilon_h(\mathbf{v}_h)|_K \in \mathbb{P}^1(K)^{3 \times 3}$ and simplifying, we have

$$\|\epsilon_{\mathcal{M}}(\Upsilon_h^2 \mathbf{v}_h) - \epsilon_h(\mathbf{v}_h)\|_{L^2(K)} \lesssim \mathbb{S}_K(\mathbf{v}_h, \mathbf{v}_h)^{1/2}.$$

Using a triangle inequality, squaring and summing over $K \in \mathcal{M}$ yields

$$\|\epsilon_{\mathcal{M}}(\Upsilon_h^2 \mathbf{v}_h)\|_{L^2(\Omega)}^2 \lesssim \|\epsilon_h(\mathbf{v}_h)\|_{L^2(\Omega)}^2 + \sum_{K \in \mathcal{M}} \mathbb{S}_K(\mathbf{v}_h, \mathbf{v}_h). \quad (5.9)$$

Let $\sigma = K|L \in \mathcal{F}^{\text{int}} \setminus \mathcal{F}_{\Gamma}$. Since σ is not a fracture face, the cells K and L are on the same side of the fracture and hence all the degrees of freedom on σ are common to K and L , and so $\Upsilon_{K\sigma}^2 \mathbf{v}_h = \Upsilon_{L\sigma}^2 \mathbf{v}_h$. Hence,

$$|\llbracket \Upsilon_h^2 \mathbf{v}_h \rrbracket|_{\sigma} = |\Upsilon_K^2 \mathbf{v}_h - \Upsilon_L^2 \mathbf{v}_h| = |(\Upsilon_K^2 \mathbf{v}_h - \Upsilon_{K\sigma}^2 \mathbf{v}_h) - (\Upsilon_L^2 \mathbf{v}_h - \Upsilon_{L\sigma}^2 \mathbf{v}_h)|. \quad (5.10)$$

For $\sigma \in \mathcal{F}^{\text{ext}} \cap \mathcal{F}_K$, we have $\mathbf{v}_{\mathcal{K}s} = \mathbf{v}_{\mathcal{K}e} = \mathbf{0}$ for all $s \in \mathcal{V}_{\sigma}$ and $e \in \mathcal{E}_{\sigma}$. Additionally since $\mathbf{v}_{K\sigma} = \mathbf{0}$, it follows that $\Upsilon_{K\sigma}^2 \mathbf{v}_h = \mathbf{0}$. Thus

$$|\llbracket \Upsilon_h^2 \mathbf{v}_h \rrbracket|_{\sigma} = |\Upsilon_K^2 \mathbf{v}_h - \Upsilon_{K\sigma}^2 \mathbf{v}_h|. \quad (5.11)$$

Taking the $L^2(\sigma)$ -norms of (5.10) and (5.11), using triangle inequalities, summing over $\sigma \in \mathcal{F} \setminus \mathcal{F}_{\Gamma}$, invoking the definition (3.6) of $\mathbb{S}_K(\cdot, \cdot)$ and using the mesh regularity to write $h_{\sigma} \simeq h_K$ whenever $\sigma \in \mathcal{F}_K$, we conclude

$$\sum_{\sigma \in \mathcal{F} \setminus \mathcal{F}_{\Gamma}} h_{\sigma}^{-1} |\llbracket \Upsilon_h^2 \mathbf{v}_h \rrbracket|_{L^2(\sigma)}^2 \lesssim \sum_{K \in \mathcal{M}} \sum_{\sigma \in \mathcal{F}_K} h_{\sigma}^{-1} \|\Upsilon_K^2 \mathbf{v}_h - \Upsilon_{K\sigma}^2 \mathbf{v}_h\|_{L^2(\sigma)}^2 \lesssim \sum_{K \in \mathcal{M}} \mathbb{S}_K(\mathbf{v}_h, \mathbf{v}_h). \quad (5.12)$$

The inequality (3.8) follows from (5.8), (5.9), and (5.12). \square

5.2 Proof of the discrete inf-sup condition

The proof of the inf-sup condition requires to interpolate displacements with minimal $H^1(\Omega \setminus \Gamma)$ regularity. To do so, we therefore first describe a Clément-like (averaged) interpolator for such displacements.

For each $K \in \mathcal{M}$ and $s \in \mathcal{V}_K$, we take an open set $U_{\mathcal{K}s} \subset \bigcup_{K \in \mathcal{K}s} K$ and a function $\bar{\omega}_{\mathcal{K}s} \in L^{\infty}(U_{\mathcal{K}s})$ such that

$$\begin{aligned} |U_{\mathcal{K}s}| &\gtrsim \max_{K \in \mathcal{K}s} |K|, & |\bar{\omega}_{\mathcal{K}s}| &\lesssim 1, \\ \frac{1}{|U_{\mathcal{K}s}|} \int_{U_{\mathcal{K}s}} \bar{\omega}_{\mathcal{K}s} &= 1, & \frac{1}{|U_{\mathcal{K}s}|} \int_{U_{\mathcal{K}s}} \mathbf{x} \bar{\omega}_{\mathcal{K}s} &= \mathbf{x}_s. \end{aligned} \quad (5.13)$$

We refer to [32, Appendix A] for an explicit construction of $(U_{\mathcal{K}s}, \bar{\omega}_{\mathcal{K}s})$ in the generic case. The averaged interpolate $\mathbb{I}_h^{\alpha} \mathbf{v} \in \mathbf{X}_{\text{grad},h}^{\alpha}$ of $\mathbf{v} \in H_0^1(\Omega \setminus \Gamma)^3$ is then defined by:

$$(\mathbb{I}_h^{\alpha} \mathbf{v})_{\mathcal{K}s} = (\mathbb{I}_h^{\alpha} \mathbf{v})_{\mathcal{K}e} = (\mathbb{I}_h^{\alpha} \mathbf{v})_{K\sigma} = \mathbf{0} \quad \forall s \in \mathcal{V}^{\text{ext}}, e \in \mathcal{E}^{\text{ext}}, \sigma \in \mathcal{F}^{\text{ext}},$$

$$\begin{aligned} (\mathbb{I}_h^a \mathbf{v})_{\mathcal{K}_s} &= \frac{1}{|U_{\mathcal{K}_s}|} \int_{U_{\mathcal{K}_s}} \bar{\omega}_{\mathcal{K}_s} \mathbf{v} & \forall s \in \mathcal{V}^{\text{int}}, \\ (\mathbb{I}_h^a \mathbf{v})_{\mathcal{K}_e} &= \frac{1}{2|U_{\mathcal{K}_{s_1}}|} \int_{U_{\mathcal{K}_{s_1}}} \bar{\omega}_{\mathcal{K}_{s_1}} \mathbf{v} + \frac{1}{2|U_{\mathcal{K}_{s_2}}|} \int_{U_{\mathcal{K}_{s_2}}} \bar{\omega}_{\mathcal{K}_{s_2}} \mathbf{v} & \forall e \in \mathcal{E}^{\text{int}}, e = [s_1, s_2], \end{aligned} \quad (5.14a)$$

$$(\mathbb{I}_h^a \mathbf{v})_{\mathcal{K}_\sigma} = \frac{1}{|\sigma|} \int_\sigma \mathbf{v}|_K \quad \forall \sigma \in \mathcal{F}^{\text{int}}, \quad (5.14b)$$

$$(\mathbb{I}_h^a \mathbf{v})_K = \Pi_K^0 \mathbf{v} \quad \forall K \in \mathcal{M}.$$

The averaged interpolator $\mathbb{I}^a : H_0^1(\Omega \setminus \Gamma)^3 \rightarrow \mathbf{X}_{\text{grad},h}$ is needed since, unlike \mathbb{I}_h , it is well-defined for functions of minimal $H^1(\Omega \setminus \Gamma)$ regularity (for which pointwise evaluation is not available). Its construction using local weighted averages over patches $U_{\mathcal{K}_s}$ lying only on one side of Γ ensures that these averages avoid the jumps of the interpolated displacement. Its two key properties used in the proof of Theorem 3.2 are: (i) exact recovery of the duality pairing, i.e., $\int_\Gamma \boldsymbol{\lambda}_h \cdot [\mathbb{I}_h^a \mathbf{v}]_h = \boldsymbol{\lambda}_h \cdot [\mathbf{v}]$ for all $\boldsymbol{\lambda}_h \in \mathbf{M}_h$; and (ii) uniform continuity for the $H^1(\Omega \setminus \Gamma)$ norm, proved in the next theorem.

Proposition 5.3 (Stability of the averaged interpolator). *For $\mathbf{v} \in H_0^1(\Omega \setminus \Gamma)^3$, it holds*

$$\|\mathbb{I}_h^a \mathbf{v}\|_{1,h} \lesssim \|\nabla \mathbf{v}\|_{L^2(\Omega)}. \quad (5.15)$$

Proof. Let $\mathbf{v} \in H_0^1(\Omega \setminus \Gamma)^3$ and $K \in \mathcal{M}$. Let

$$\mathcal{N}(K) := \bigcup_{s \in \mathcal{V}_K} \bigcup_{L \in \mathcal{K}_s} L$$

be the patch around K made of all the cells in \mathcal{K}_s for each s vertex of K . By definition of \mathcal{K}_s , we have $\mathbf{v} \in H^1(\mathcal{N}(K))^3$. Denote by \mathbf{q} the $L^2(\mathcal{N}(K))^3$ -projection of \mathbf{v} on $\mathbb{P}^1(\mathcal{N}(K))^3$. This projection enjoys the following approximation and stability properties [25, Theorem 1.45]:

$$\|\mathbf{q} - \mathbf{v}\|_{L^2(\mathcal{N}(K))} \lesssim h_K \|\nabla \mathbf{v}\|_{L^2(\mathcal{N}(K))}, \quad (5.16)$$

$$\|(\mathbf{q} - \mathbf{v})|_K\|_{L^2(\sigma)} \lesssim h_K^{1/2} \|\nabla \mathbf{v}\|_{L^2(\mathcal{N}(K))} \quad \forall \sigma \in \mathcal{F}_K, \quad (5.17)$$

$$\|\nabla \mathbf{q}\|_{L^2(\mathcal{N}(K))} \lesssim \|\nabla \mathbf{v}\|_{L^2(\mathcal{N}(K))}. \quad (5.18)$$

Recalling [26, Lemma 3] and from Lemma 4.1 we have $\Upsilon_{Ke}^2 \mathbb{I}_h \mathbf{q} = \mathbf{q}$, $\Upsilon_{K\sigma}^2 \mathbb{I}_h \mathbf{q} = \mathbf{q}$, $\mathbb{G}_K^1 \mathbb{I}_h \mathbf{q} = \nabla \mathbf{q}$, and $\Upsilon_K^2 \mathbb{I}_h \mathbf{q} = \mathbf{q}$. Thus, the definition (3.6) of $\mathbb{S}_K(\cdot, \cdot)$ gives

$$\mathbb{S}_K(\mathbb{I}_h \mathbf{q}, \underline{\mathbf{w}}_h) = 0 \quad \forall \underline{\mathbf{w}}_h \in \mathbf{X}_{\text{grad},h}. \quad (5.19)$$

The definition (3.7) of $\|\cdot\|_{1,K}$, then gives

$$\|\mathbb{I}_h \mathbf{q}\|_{1,K} = \|\nabla \mathbf{q}\|_{L^2(K)} \lesssim \|\nabla \mathbf{v}\|_{L^2(\mathcal{N}(K))}. \quad (5.20)$$

To prove (5.15), we bound each type of degree of freedom (vertex, edge, face, element), then use (5.6) to conclude.

From [26, Proposition 5.5], for any $s \in \mathcal{V}_K$ the following inequality holds:

$$|(\mathbb{I}_h \mathbf{q})_{\mathcal{K}_s} - (\mathbb{I}_h^a \mathbf{v})_{\mathcal{K}_s}| \lesssim h_K^{-1/2} \|\nabla \mathbf{v}\|_{L^2(\mathcal{N}(K))}. \quad (5.21)$$

If $e \in \mathcal{E}_K^{\text{ext}}$, then $(\mathbb{I}_h^a \mathbf{v})_{\mathcal{K}_e} = \mathbf{0}$ and $(\mathbb{I}_h \mathbf{q})_{\mathcal{K}_e} = \Pi_e^0(\mathbf{q})$. Take $\sigma \in \mathcal{F}^{\text{ext}}$ that contains e and write

$$|(\mathbb{I}_h \mathbf{q})_{\mathcal{K}_e} - (\mathbb{I}_h^a \mathbf{v})_{\mathcal{K}_e}| = |\Pi_e^0(\mathbf{q})| \leq \|\mathbf{q}\|_{L^\infty(e)} \leq \|\mathbf{q}\|_{L^\infty(\sigma)} \lesssim h_\sigma^{-1} \|\mathbf{q}\|_{L^2(\sigma)}$$

$$\lesssim h_\sigma^{-1} h_K^{1/2} \|\nabla \mathbf{q}\|_{L^2(\mathcal{N}(K))} \lesssim h_K^{-1/2} \|\nabla \mathbf{v}\|_{L^2(\mathcal{N}(K))},$$

where we have used the definition of interpolation in the first inequality, the inverse Lebesgue inequality [25, Lemma 1.25] for the third inequality, the discrete trace inequality [25, Lemma 1.32] in the fourth inequality, and the mesh regularity assumption (to write $h_K \approx h_\sigma$) along with (5.18) in the last inequality.

If $e = [s_1, s_2] \in \mathcal{E}_K^{\text{int}}$, then (5.13), (5.14a), and the fact that \mathbf{q} is linear ensure that

$$(\mathbb{I}_h \mathbf{q})_{\mathcal{K}e} = \Pi_e^0(\mathbf{q}) = \frac{1}{2|U_{\mathcal{K}s_1}|} \int_{U_{\mathcal{K}s_1}} \bar{\omega}_{\mathcal{K}s_1} \mathbf{q} + \frac{1}{2|U_{\mathcal{K}s_2}|} \int_{U_{\mathcal{K}s_2}} \bar{\omega}_{\mathcal{K}s_2} \mathbf{q}.$$

Hence

$$\begin{aligned} |(\mathbb{I}_h \mathbf{q})_{\mathcal{K}e} - (\mathbb{I}_h^a \mathbf{v})_{\mathcal{K}e}| &= \left| \sum_{j=1}^2 \frac{1}{2|U_{\mathcal{K}s_j}|} \int_{U_{\mathcal{K}s_j}} \bar{\omega}_{\mathcal{K}s_j} (\mathbf{q} - \mathbf{v}) \right| \\ &\lesssim \sum_{j=1}^2 |U_{\mathcal{K}s_j}|^{-1/2} \|\mathbf{q} - \mathbf{v}\|_{L^2(U_{\mathcal{K}s_j})} \lesssim h_K^{-1/2} \|\nabla \mathbf{v}\|_{L^2(\mathcal{N}(K))}, \end{aligned}$$

where the first inequality follows from the bound $|\bar{\omega}_{\mathcal{K}s_j}| \lesssim 1$ and the Cauchy–Schwarz inequality, while the conclusion is obtained using $|U_{\mathcal{K}s_j}| \gtrsim |K|$, $U_{\mathcal{K}s_j} \subset \mathcal{N}(K)$, and (5.16).

If $\sigma \in \mathcal{F}_K^{\text{ext}}$, then $(\mathbb{I}_h^a \mathbf{v})_{\mathcal{K}\sigma} = \mathbf{0}$ and $(\mathbb{I}_h \mathbf{q})_{\mathcal{K}\sigma} = \Pi_\sigma^0(\mathbf{q})$, so

$$|(\mathbb{I}_h \mathbf{q})_{\mathcal{K}\sigma} - (\mathbb{I}_h^a \mathbf{v})_{\mathcal{K}\sigma}| = |\Pi_\sigma^0(\mathbf{q})| \leq \|\mathbf{q}\|_{L^\infty(\sigma)} \lesssim h_K^{-1/2} \|\nabla \mathbf{v}\|_{L^2(\mathcal{N}(K))}.$$

If $\sigma \in \mathcal{F}_K^{\text{int}}$, then

$$|(\mathbb{I}_h \mathbf{q})_{\mathcal{K}\sigma} - (\mathbb{I}_h^a \mathbf{v})_{\mathcal{K}\sigma}| = \left| \frac{1}{|\sigma|} \int_\sigma (\mathbf{q} - \mathbf{v})|_K \right| \lesssim |h_\sigma|^{-1} \|\mathbf{q} - \mathbf{v}\|_{L^2(\sigma)} \stackrel{(5.17)}{\lesssim} h_K^{-1/2} \|\nabla \mathbf{v}\|_{L^2(\mathcal{N}(K))}.$$

Finally, for the cell degree of freedom, we write

$$|(\mathbb{I}_h \mathbf{q})_K - (\mathbb{I}_h^a \mathbf{v})_K| = \left| \frac{1}{|K|} \int_K \mathbf{q} - \mathbf{v} \right| \lesssim |h_K|^{-3/2} \|\mathbf{q} - \mathbf{v}\|_{L^2(K)} \stackrel{(5.16)}{\lesssim} h_K^{-1/2} \|\nabla \mathbf{v}\|_{L^2(\mathcal{N}(K))}. \quad (5.22)$$

Gathering (5.21)–(5.22) and invoking the bound (5.6) with $\underline{\mathbf{w}}_h = \mathbb{I}_h \mathbf{q} - \mathbb{I}_h^a \mathbf{v}$ yields

$$\|\mathbb{I}_h \mathbf{q} - \mathbb{I}_h^a \mathbf{v}\|_{1,K} \lesssim \|\nabla \mathbf{v}\|_{L^2(\mathcal{N}(K))}. \quad (5.23)$$

Combining (5.20) and (5.23), squaring, summing over $K \in \mathcal{M}$ and gathering the integrals by cells and using the mesh regularity to see that $\#\{K \in \mathcal{M} : L \in \mathcal{N}_K\} \lesssim 1$ for all $L \in \mathcal{M}$, we infer

$$\|\mathbb{I}_h^a \mathbf{v}\|_{1,h}^2 \lesssim \sum_{K \in \mathcal{M}} \|\nabla \mathbf{v}\|_{L^2(\mathcal{N}(K))}^2 \lesssim \|\nabla \mathbf{v}\|_{L^2(\Omega)}^2. \quad \square$$

With the establishment of Proposition 5.3, we are now ready to prove the discrete inf-sup condition (Theorem 3.2).

Proof of Theorem 3.2: Let $\lambda_h \in \mathbf{M}_h$. Recalling the definition (3.11) of the $H^{-1/2}$ -like norm, it suffices to prove that for each $\mathbf{v} \in H_0^1(\Omega \setminus \Gamma)^3$, there exists some $\underline{\mathbf{v}}_h \in \mathbf{X}_{\text{grad},h,0}$ such that

$$\frac{\int_{\Gamma} \lambda_h \cdot \llbracket \underline{\mathbf{v}}_h \rrbracket_h}{\|\underline{\mathbf{v}}_h\|_{1,h}} \gtrsim \frac{\int_{\Gamma} \lambda_h \cdot \llbracket \mathbf{v} \rrbracket}{\|\mathbf{v}\|_{H^1(\Omega \setminus \Gamma)}}. \quad (5.24)$$

Let us consider $\underline{\mathbf{v}}_h = \mathbb{I}_h^a \mathbf{v}$ with the interpolator defined by (5.14). Since λ_h is piecewise constant on \mathcal{F}_{Γ} , we have

$$\int_{\Gamma} \lambda_h \cdot \llbracket \underline{\mathbf{v}}_h \rrbracket_h = \sum_{\sigma \in \mathcal{F}_{\Gamma}} \int_{\sigma} \lambda_h \cdot \llbracket \mathbb{I}_h^a \mathbf{v} \rrbracket_{\sigma} \stackrel{(3.2),(4.3),(5.14b)}{=} \sum_{\sigma \in \mathcal{F}_{\Gamma}} \int_{\sigma} \lambda_h \cdot \llbracket \mathbf{v} \rrbracket = \int_{\Gamma} \lambda_h \cdot \llbracket \mathbf{v} \rrbracket.$$

Dividing throughout by $\|\underline{\mathbf{v}}_h\|_{1,h} = \|\mathbb{I}_h^a \mathbf{v}\|_{1,h}$ and using (5.15) to infer that $\|\mathbb{I}_h^a \mathbf{v}\|_{1,h} \lesssim \|\mathbf{v}\|_{H^1(\Omega \setminus \Gamma)}$ proves (5.24). \square

5.3 Proof of abstract error bounds

To derive the abstract error bound in Theorem 4.2, we need to establish the following lemmas.

Lemma 5.4 (Bound on the discrete stress). *For all $\underline{\mathbf{v}}_h \in \mathbf{X}_{\text{grad},h,0}$, it holds:*

$$\|\boldsymbol{\sigma}_h(\underline{\mathbf{v}}_h)\|_{L^2(\Omega)} \lesssim \sqrt{\mu_2} \left(1 + \left(\frac{\nu}{1-2\nu} \right)^{\frac{1}{2}} \right) \|\underline{\mathbf{v}}_h\|_{\text{en},h}, \quad (5.25)$$

where the hidden constant in \lesssim is independent of E and ν .

Proof. First, recall the definition of $\boldsymbol{\sigma}_h(\cdot)$ from (3.4) to get

$$\boldsymbol{\sigma}_h(\underline{\mathbf{v}}_h) = \frac{E}{1+\nu} \left(\boldsymbol{\epsilon}_h(\underline{\mathbf{v}}_h) + \frac{\nu}{1-2\nu} \text{div}_h(\underline{\mathbf{v}}_h) \mathbf{I}_3 \right).$$

An application of the triangle inequality in the above equation leads to

$$\|\boldsymbol{\sigma}_h(\underline{\mathbf{v}}_h)\|_{L^2(\Omega)} \lesssim \frac{E}{1+\nu} \left(\|\boldsymbol{\epsilon}_h(\underline{\mathbf{v}}_h)\|_{L^2(\Omega)} + \frac{\nu}{1-2\nu} \|\text{div}_h(\underline{\mathbf{v}}_h)\|_{L^2(\Omega)} \right). \quad (5.26)$$

The definition of $\|\cdot\|_{\text{en},h}$ from (3.9) and using $(a+b)^{1/2} \geq \frac{1}{2}(a^{1/2} + b^{1/2})$, we have

$$\|\underline{\mathbf{v}}_h\|_{\text{en},h} \geq \frac{1}{2} \left(\frac{E}{1+\nu} \right)^{\frac{1}{2}} \left(\|\boldsymbol{\epsilon}_h(\underline{\mathbf{v}}_h)\|_{L^2(\Omega)} + \left(\frac{\nu}{1-2\nu} \right)^{\frac{1}{2}} \|\text{div}_h(\underline{\mathbf{v}}_h)\|_{L^2(\Omega)} \right),$$

which gives

$$\|\boldsymbol{\epsilon}_h(\underline{\mathbf{v}}_h)\|_{L^2(\Omega)} + \left(\frac{\nu}{1-2\nu} \right)^{\frac{1}{2}} \|\text{div}_h(\underline{\mathbf{v}}_h)\|_{L^2(\Omega)} \lesssim \left(\frac{E}{1+\nu} \right)^{-\frac{1}{2}} \|\underline{\mathbf{v}}_h\|_{\text{en},h}.$$

Plugging this relation into (5.26) leads to

$$\|\boldsymbol{\sigma}_h(\underline{\mathbf{v}}_h)\|_{L^2(\Omega)} \lesssim \left(\frac{E}{1+\nu} \right)^{\frac{1}{2}} \left(1 + \left(\frac{\nu}{1-2\nu} \right)^{\frac{1}{2}} \right) \|\underline{\mathbf{v}}_h\|_{\text{en},h},$$

The above inequality with $\frac{E}{1+\nu} \leq \mu_2$ implies (5.25). \square

Lemma 5.5 (Fortin interpolator). *Let $K \in \mathcal{M}$ and $\boldsymbol{\xi} \in \mathbb{P}^1(K)^{3 \times 3}$. Then, we have*

$$\int_K (\operatorname{div}(\mathbf{u}) - \operatorname{div}_h(\mathbb{I}_h \mathbf{u})) \mathbf{I}_3 : \boldsymbol{\xi} = 0.$$

Consequently,

$$\int_\Omega (\boldsymbol{\sigma}(\mathbf{u}) - \boldsymbol{\sigma}_h(\mathbb{I}_h \mathbf{u})) : \boldsymbol{\xi} = \frac{E}{1 + \nu} \int_\Omega (\boldsymbol{\epsilon}(\mathbf{u}) - \boldsymbol{\epsilon}_h(\mathbb{I}_h \mathbf{u})) : \boldsymbol{\xi}. \quad (5.27)$$

Proof. Let $\boldsymbol{\xi} \in \mathbb{P}^1(K)^{3 \times 3}$. We have $\operatorname{tr} \boldsymbol{\xi} \in \mathbb{P}^1(K)$. Thus,

$$\begin{aligned} \int_K (\operatorname{tr} \boldsymbol{\epsilon}(\mathbf{u}) - \operatorname{div}_h(\mathbb{I}_h \mathbf{u})) \mathbf{I}_3 : \boldsymbol{\xi} &= \int_K (\operatorname{tr} \boldsymbol{\epsilon}(\mathbf{u}) - \operatorname{tr} \boldsymbol{\epsilon}_h(\mathbb{I}_h \mathbf{u})) \operatorname{tr} \boldsymbol{\xi} \\ &= \int_K (\boldsymbol{\epsilon}(\mathbf{u}) - \boldsymbol{\epsilon}_h(\mathbb{I}_h \mathbf{u})) : (\operatorname{tr} \boldsymbol{\xi}) \mathbf{I}_3 = \int_K (\nabla \mathbf{u} - \mathbb{G}_h^1(\mathbb{I}_h \mathbf{u})) : (\operatorname{tr} \boldsymbol{\xi}) \mathbf{I}_3 \\ &\stackrel{\text{IBP}, (3.3), (4.1b)}{=} \sum_{\sigma \in \mathcal{F}_K} \int_\sigma \mathbf{u}|_K \cdot (\operatorname{tr} \boldsymbol{\xi}) \mathbf{n}_{K\sigma} - \int_K \mathbf{u} \cdot \operatorname{div}((\operatorname{tr} \boldsymbol{\xi}) \mathbf{I}_3) + \int_K (\Pi_K^0 \mathbf{u} + \tilde{\mathbf{u}}_K) \cdot \operatorname{div}((\operatorname{tr} \boldsymbol{\xi}) \mathbf{I}_3) \\ &\quad - \sum_{\sigma \in \mathcal{F}_K} \int_\sigma \Upsilon_{K\sigma}^2 \mathbb{I}_h \mathbf{u} \cdot (\operatorname{tr} \boldsymbol{\xi}) \mathbf{n}_{K\sigma} \\ &= \int_K (\cancel{\Pi_K^0 \mathbf{u} - \mathbf{u}}) \cdot \operatorname{div}((\operatorname{tr} \boldsymbol{\xi}) \mathbf{I}_3) + \int_K \tilde{\mathbf{u}}_K \cdot \operatorname{div}((\operatorname{tr} \boldsymbol{\xi}) \mathbf{I}_3) \\ &\quad + \sum_{\sigma \in \mathcal{F}_K} \int_\sigma (\mathbf{u}|_K - \Upsilon_{K\sigma}^2 \mathbb{I}_h \mathbf{u}) \cdot (\operatorname{tr} \boldsymbol{\xi}) \mathbf{n}_{K\sigma} = 0, \end{aligned}$$

where the cancellation in the fifth equation is justified by the definition of Π_K^0 and $\operatorname{div}((\operatorname{tr} \boldsymbol{\xi}) \mathbf{I}_3) \in \mathbb{P}^0(K)^3$ while, in the conclusion, we have used the definition (4.2) of $\tilde{\mathbf{u}}_K$ with $\phi = \operatorname{tr} \boldsymbol{\xi}$, after noticing that $\operatorname{div}((\operatorname{tr} \boldsymbol{\xi}) \mathbf{I}_3) = \nabla \operatorname{tr} \boldsymbol{\xi}$. \square

Lemma 5.6 (L^2 -to- $H^{-1/2}$ projection stability). *Let $\boldsymbol{\chi} \in L^2(\Gamma)^3$. Then, we have*

$$\|\boldsymbol{\chi} - \Pi_{\mathcal{F}_\Gamma}^0 \boldsymbol{\chi}\|_{-1/2, \Gamma} \lesssim h^{1/2} \|\boldsymbol{\chi} - \Pi_{\mathcal{F}_\Gamma}^0 \boldsymbol{\chi}\|_{L^2(\Gamma)}.$$

Proof. Let $\mathbf{v} \in H_0^1(\Omega \setminus \Gamma)^3 \setminus \{0\}$. Then,

$$\begin{aligned} \sum_{\sigma \in \mathcal{F}_\Gamma} \|[\mathbf{v}] - \Pi_\sigma^0 [\mathbf{v}]\|_{L^2(\sigma)} &\leq \sum_{\sigma \in \mathcal{F}_\Gamma} \sum_{K \in \mathcal{M}_\sigma} \|\mathbf{v}|_K - \Pi_\sigma^0(\mathbf{v}|_K)\|_{L^2(\sigma)} \\ &= \sum_{\sigma \in \mathcal{F}_\Gamma} \sum_{K \in \mathcal{M}_\sigma} \|\mathbf{v}|_K - \Pi_K^0 \mathbf{v} - \Pi_\sigma^0(\mathbf{v}|_K - \Pi_K^0 \mathbf{v})\|_{L^2(\sigma)} \\ &\leq \sum_{\sigma \in \mathcal{F}_\Gamma} \sum_{K \in \mathcal{M}_\sigma} 2 \|\mathbf{v}|_K - \Pi_K^0 \mathbf{v}\|_{L^2(\sigma)} \\ &\lesssim \sum_{\sigma \in \mathcal{F}_\Gamma} h_\sigma^{1/2} \sum_{K \in \mathcal{M}_\sigma} \|\mathbf{v}\|_{H^1(K)} \lesssim h^{1/2} \|\mathbf{v}\|_{H^1(\Omega \setminus \Gamma)}. \end{aligned}$$

In deriving these estimates, we invoke the definition of $[\mathbf{v}]$ and triangle inequalities (first line), use $\Pi_\sigma^0(\Pi_K^0 \mathbf{v}) = \Pi_K^0 \mathbf{v}$ since $(\Pi_K^0 \mathbf{v})|_\sigma \in \mathbb{P}^0(\sigma)^3$ (second line), apply the triangle inequality together with the $L^2(\sigma)$ -boundedness of Π_σ^0 (third line), and the approximation properties of Π_K^0 given in

[25, Theorem 1.45] (fourth line). Now, using orthogonality of the projection operator $\Pi_{\mathcal{F}_\Gamma}^0$, the Cauchy-Schwarz inequality, and the previous bound, we conclude

$$\begin{aligned} \int_{\Gamma} (\boldsymbol{\chi} - \Pi_{\mathcal{F}_\Gamma}^0 \boldsymbol{\chi}) \cdot \llbracket \mathbf{v} \rrbracket &= \int_{\Gamma} (\boldsymbol{\chi} - \Pi_{\mathcal{F}_\Gamma}^0 \boldsymbol{\chi}) \cdot (\llbracket \mathbf{v} \rrbracket - \Pi_{\mathcal{F}_\Gamma}^0 \llbracket \mathbf{v} \rrbracket) \\ &\lesssim \|\boldsymbol{\chi} - \Pi_{\mathcal{F}_\Gamma}^0 \boldsymbol{\chi}\|_{L^2(\Gamma)} \left(\sum_{\sigma \in \mathcal{F}_\Gamma} \|\llbracket \mathbf{v} \rrbracket - \Pi_{\sigma}^0 \llbracket \mathbf{v} \rrbracket\|_{L^2(\sigma)} \right) \\ &\lesssim h^{1/2} \|\boldsymbol{\chi} - \Pi_{\mathcal{F}_\Gamma}^0 \boldsymbol{\chi}\|_{L^2(\Gamma)} \|\mathbf{v}\|_{H^1(\Omega \setminus \Gamma)}. \end{aligned}$$

The lemma follows from Definition 3.1. \square

Proof of Theorem 4.2: We first notice that the regularity assumption ensures that $\mathbf{u} \in C_0^0(\bar{\Omega} \setminus \Gamma)^3$. Let us start by estimating the norm of $\underline{\mathbf{u}}_h - \mathbb{I}_h \mathbf{u}$. By definition (3.9) of the inner product corresponding to $\|\cdot\|_{\text{en},h}$, we have

$$\begin{aligned} \|\underline{\mathbf{u}}_h - \mathbb{I}_h \mathbf{u}\|_{\text{en},h}^2 &= \int_{\Omega} \boldsymbol{\sigma}_h(\underline{\mathbf{u}}_h - \mathbb{I}_h \mathbf{u}) : \boldsymbol{\epsilon}_h(\underline{\mathbf{u}}_h - \mathbb{I}_h \mathbf{u}) + \mu_1 \mathbb{S}_h(\underline{\mathbf{u}}_h - \mathbb{I}_h \mathbf{u}, \underline{\mathbf{u}}_h - \mathbb{I}_h \mathbf{u}) \\ &\stackrel{(3.5a)}{=} \sum_{K \in \mathcal{M}} \int_K \mathbf{f} \cdot (\mathbf{u}_K - \mathbb{I}_K \mathbf{u}) - \int_{\Gamma} \boldsymbol{\lambda}_h \cdot \llbracket \underline{\mathbf{u}}_h - \mathbb{I}_h \mathbf{u} \rrbracket_h \\ &\quad - \int_{\Omega} \boldsymbol{\sigma}_h(\mathbb{I}_h \mathbf{u}) : \boldsymbol{\epsilon}_h(\underline{\mathbf{u}}_h - \mathbb{I}_h \mathbf{u}) - \mu_1 \mathbb{S}_h(\mathbb{I}_h \mathbf{u}, \underline{\mathbf{u}}_h - \mathbb{I}_h \mathbf{u}). \end{aligned} \quad (5.28)$$

The definition (4.9) of w_h together with $\mathbf{f} = -\text{div}(\boldsymbol{\sigma}(\mathbf{u}))$ and $\boldsymbol{\lambda} = -\gamma_{\mathbf{n}}^+ \boldsymbol{\sigma}(\mathbf{u})$ yields

$$\begin{aligned} 0 &= w_h(\boldsymbol{\sigma}(\mathbf{u}), \underline{\mathbf{u}}_h - \mathbb{I}_h \mathbf{u}) - \sum_{K \in \mathcal{M}} \int_K \mathbf{f} \cdot (\mathbf{u}_K - \mathbb{I}_K \mathbf{u}) + \int_{\Gamma} \Pi_{\mathcal{F}_\Gamma}^0 \boldsymbol{\lambda} \cdot \llbracket \underline{\mathbf{u}}_h - \mathbb{I}_h \mathbf{u} \rrbracket_h \\ &\quad + \int_{\Omega} \boldsymbol{\sigma}(\mathbf{u}) : \boldsymbol{\epsilon}_h(\underline{\mathbf{u}}_h - \mathbb{I}_h \mathbf{u}). \end{aligned}$$

Adding this relation to (5.28) leads to

$$\begin{aligned} \|\underline{\mathbf{u}}_h - \mathbb{I}_h \mathbf{u}\|_{\text{en},h}^2 &= w_h(\boldsymbol{\sigma}(\mathbf{u}), \underline{\mathbf{u}}_h - \mathbb{I}_h \mathbf{u}) + \int_{\Gamma} (\Pi_{\mathcal{F}_\Gamma}^0 \boldsymbol{\lambda} - \boldsymbol{\lambda}_h) \cdot \llbracket \underline{\mathbf{u}}_h - \mathbb{I}_h \mathbf{u} \rrbracket_h \\ &\quad + \int_{\Omega} (\boldsymbol{\sigma}(\mathbf{u}) - \boldsymbol{\sigma}_h(\mathbb{I}_h \mathbf{u})) : \boldsymbol{\epsilon}_h(\underline{\mathbf{u}}_h - \mathbb{I}_h \mathbf{u}) - \mu_1 \mathbb{S}_h(\mathbb{I}_h \mathbf{u}, \underline{\mathbf{u}}_h - \mathbb{I}_h \mathbf{u}) \\ &\stackrel{(4.9), (3.10), (5.27)}{\leq} \left(\frac{\tilde{C}}{\mu_1} \right)^{\frac{1}{2}} \|\underline{\mathbf{u}}_h - \mathbb{I}_h \mathbf{u}\|_{\text{en},h} \mathcal{W}_h(\boldsymbol{\sigma}(\mathbf{u})) - \int_{\Gamma} (\Pi_{\mathcal{F}_\Gamma}^0 \boldsymbol{\lambda} - \boldsymbol{\lambda}_h) \cdot \llbracket \mathbb{I}_h \mathbf{u} \rrbracket_h \\ &\quad + \frac{E}{1+\nu} \int_{\Omega} (\boldsymbol{\epsilon}(\mathbf{u}) - \boldsymbol{\epsilon}_h(\mathbb{I}_h \mathbf{u})) : \boldsymbol{\epsilon}_h(\underline{\mathbf{u}}_h - \mathbb{I}_h \mathbf{u}) - \mu_1 \mathbb{S}_h(\mathbb{I}_h \mathbf{u}, \underline{\mathbf{u}}_h - \mathbb{I}_h \mathbf{u}), \end{aligned} \quad (5.29)$$

where in the last inequality we have used that $\boldsymbol{\epsilon}_K(\underline{\mathbf{u}}_h - \mathbb{I}_h \mathbf{u}) \in \mathbb{P}^1(K)^{3 \times 3}$ for all $K \in \mathcal{M}$ and, since $\Pi_{\mathcal{F}_\Gamma}^0 \boldsymbol{\lambda} \in \mathcal{C}_{f,h}$, the relation (3.5b) to write $\int_{\Gamma} (\Pi_{\mathcal{F}_\Gamma}^0 \boldsymbol{\lambda} - \boldsymbol{\lambda}_h) \cdot \llbracket \underline{\mathbf{u}}_h \rrbracket_h \leq 0$. Using the Cauchy-Schwarz inequality on the last two terms, and Young's inequality ($ab \leq a^2 + b^2/4$), we get

$$\left(\frac{\tilde{C}}{\mu_1} \right)^{1/2} \|\underline{\mathbf{u}}_h - \mathbb{I}_h \mathbf{u}\|_{\text{en},h} \mathcal{W}_h(\boldsymbol{\sigma}(\mathbf{u})) \leq \frac{\tilde{C}}{\mu_1} \mathcal{W}_h(\boldsymbol{\sigma}(\mathbf{u}))^2 + \frac{1}{4} \|\underline{\mathbf{u}}_h - \mathbb{I}_h \mathbf{u}\|_{\text{en},h}^2$$

while, for the stabilisation term,

$$\begin{aligned} |\mu_1 \mathcal{S}_h(\mathbb{I}_h \mathbf{u}, \underline{\mathbf{u}}_h - \mathbb{I}_h \mathbf{u})| &\leq \mu_1 \mathcal{S}_h(\mathbb{I}_h \mathbf{u}, \mathbb{I}_h \mathbf{u}) + \frac{\mu_1}{4} \mathcal{S}_h(\underline{\mathbf{u}}_h - \mathbb{I}_h \mathbf{u}, \underline{\mathbf{u}}_h - \mathbb{I}_h \mathbf{u}) \\ &\stackrel{\mu_1 \leq \mu_2}{\leq} \mu_2 \mathcal{S}_h(\mathbb{I}_h \mathbf{u}, \mathbb{I}_h \mathbf{u}) + \frac{\mu_1}{4} \mathcal{S}_h(\underline{\mathbf{u}}_h - \mathbb{I}_h \mathbf{u}, \underline{\mathbf{u}}_h - \mathbb{I}_h \mathbf{u}), \end{aligned}$$

and, for the symmetric gradient term,

$$\begin{aligned} &\left| \frac{E}{1+\nu} \int_{\Omega} (\boldsymbol{\epsilon}(\mathbf{u}) - \boldsymbol{\epsilon}_h(\mathbb{I}_h \mathbf{u})) : \boldsymbol{\epsilon}_h(\underline{\mathbf{u}}_h - \mathbb{I}_h \mathbf{u}) \right| \\ &\leq \frac{E}{1+\nu} \left(\|\boldsymbol{\epsilon}(\mathbf{u}) - \boldsymbol{\epsilon}_h(\mathbb{I}_h \mathbf{u})\|_{L^2(\Omega)}^2 + \frac{1}{4} \|\boldsymbol{\epsilon}_h(\underline{\mathbf{u}}_h - \mathbb{I}_h \mathbf{u})\|_{L^2(\Omega)}^2 \right) \\ &\stackrel{\frac{E}{1+\nu} \leq \mu_2}{\leq} \mu_2 \|\boldsymbol{\epsilon}(\mathbf{u}) - \boldsymbol{\epsilon}_h(\mathbb{I}_h \mathbf{u})\|_{L^2(\Omega)}^2 + \frac{E}{4(1+\nu)} \|\boldsymbol{\epsilon}_h(\underline{\mathbf{u}}_h - \mathbb{I}_h \mathbf{u})\|_{L^2(\Omega)}^2. \end{aligned}$$

Plugging these three inequalities into (5.29), then using the definition (4.8) of \mathfrak{C}_h and

$$\frac{E}{4(1+\nu)} \|\boldsymbol{\epsilon}_h(\underline{\mathbf{u}}_h - \mathbb{I}_h \mathbf{u})\|_{L^2(\Omega)}^2 + \frac{\mu_1}{4} \mathcal{S}_h(\underline{\mathbf{u}}_h - \mathbb{I}_h \mathbf{u}, \underline{\mathbf{u}}_h - \mathbb{I}_h \mathbf{u}) \stackrel{(3.9)}{\leq} \frac{1}{4} \|\underline{\mathbf{u}}_h - \mathbb{I}_h \mathbf{u}\|_{\text{en},h}^2,$$

we obtain

$$\|\underline{\mathbf{u}}_h - \mathbb{I}_h \mathbf{u}\|_{\text{en},h}^2 \leq \frac{2\tilde{\mathcal{C}}}{\mu_1} \mathcal{W}_h(\boldsymbol{\sigma}(\mathbf{u}))^2 + 2\mu_2 \mathfrak{C}_h(\mathbf{u}, \mathbb{I}_h \mathbf{u})^2 - 2 \int_{\Gamma} (\Pi_{\mathcal{F}_\Gamma}^0 \boldsymbol{\lambda} - \boldsymbol{\lambda}_h) \cdot \llbracket \mathbb{I}_h \mathbf{u} \rrbracket_h. \quad (5.30)$$

Let us now consider the last addend. For all $\sigma \in \mathcal{F}_\Gamma$, the definition (3.2) of $\llbracket \cdot \rrbracket_\sigma$ gives

$$\begin{aligned} \int_{\sigma} (\Pi_{\sigma}^0 \boldsymbol{\lambda} - \boldsymbol{\lambda}_{\sigma}) \cdot \llbracket \mathbb{I}_h \mathbf{u} \rrbracket_{\sigma} &= \int_{\sigma} (\Pi_{\sigma}^0 \boldsymbol{\lambda} - \boldsymbol{\lambda}_{\sigma}) \cdot (\Upsilon_{K\sigma}^2 \mathbb{I}_h \mathbf{u} - \Upsilon_{L\sigma}^2 \mathbb{I}_h \mathbf{u}) \\ &\stackrel{(4.3), (4.1a)}{=} \int_{\sigma} (\Pi_{\sigma}^0 \boldsymbol{\lambda} - \boldsymbol{\lambda}_{\sigma}) \cdot (\Pi_{\sigma}^0(\mathbf{u}|_K) - \Pi_{\sigma}^0(\mathbf{u}|_L)) \\ &= \int_{\sigma} (\Pi_{\sigma}^0 \boldsymbol{\lambda} - \boldsymbol{\lambda}_{\sigma}) \cdot \llbracket \mathbf{u} \rrbracket, \end{aligned}$$

where the second and third equalities are further justified by $\Pi_{\sigma}^0 \boldsymbol{\lambda} - \boldsymbol{\lambda}_{\sigma} \in \mathbb{P}^0(\sigma)^3$ together with the definition of Π_{σ}^0 . Summing these equations over $\sigma \in \mathcal{F}_\Gamma$, we obtain

$$\begin{aligned} - \int_{\Gamma} (\Pi_{\mathcal{F}_\Gamma}^0 \boldsymbol{\lambda} - \boldsymbol{\lambda}_h) \cdot \llbracket \mathbb{I}_h \mathbf{u} \rrbracket_h &= \int_{\Gamma} (\boldsymbol{\lambda}_h - \Pi_{\mathcal{F}_\Gamma}^0 \boldsymbol{\lambda}) \cdot \llbracket \mathbf{u} \rrbracket \\ &= \underbrace{\int_{\Gamma} (\boldsymbol{\lambda}_h - \boldsymbol{\lambda}) \cdot \llbracket \mathbf{u} \rrbracket}_{\leq 0 \text{ by (2.2a) and } \boldsymbol{\lambda}_h \in \mathcal{C}_{f,h} \subset \mathcal{C}_f} + \int_{\Gamma} (\boldsymbol{\lambda} - \Pi_{\mathcal{F}_\Gamma}^0 \boldsymbol{\lambda}) \cdot \llbracket \mathbf{u} \rrbracket \\ &\leq \int_{\Gamma} (\boldsymbol{\lambda} - \Pi_{\mathcal{F}_\Gamma}^0 \boldsymbol{\lambda}) \cdot (\llbracket \mathbf{u} \rrbracket - \Pi_{\mathcal{F}_\Gamma}^0 \llbracket \mathbf{u} \rrbracket), \end{aligned}$$

where, in the conclusion, we have introduced $\Pi_{\mathcal{F}_\Gamma}^0 \llbracket \mathbf{u} \rrbracket$ using the definition of $\Pi_{\mathcal{F}_\Gamma}^0 \boldsymbol{\lambda}$. Plugging this upper bound into (5.30) leads to

$$\|\underline{\mathbf{u}}_h - \mathbb{I}_h \mathbf{u}\|_{\text{en},h}^2 \lesssim \frac{1}{\mu_1} \mathcal{W}_h(\boldsymbol{\sigma}(\mathbf{u}))^2 + \mu_2 \mathfrak{C}_h(\mathbf{u}, \mathbb{I}_h \mathbf{u})^2 + \int_{\Gamma} (\boldsymbol{\lambda} - \Pi_{\mathcal{F}_\Gamma}^0 \boldsymbol{\lambda}) \cdot (\llbracket \mathbf{u} \rrbracket - \Pi_{\mathcal{F}_\Gamma}^0 \llbracket \mathbf{u} \rrbracket),$$

where \lesssim absorbs the quantity $\max\{2\tilde{C}, 2\}$ which is independent from E and ν . This proves the estimate (4.10).

We now turn to the error on the Lagrange multiplier. Using the definition of w_h in (4.9) (together with $\gamma_n^+ \boldsymbol{\sigma}(\mathbf{u}) = -\boldsymbol{\lambda}$) and the scheme (3.5a), we have for all $\underline{\mathbf{w}}_h \in \mathbf{X}_{\text{grad},h,0}$:

$$\begin{aligned}
& \int_{\Gamma} (\Pi_{\mathcal{F}_T}^0 \boldsymbol{\lambda} - \boldsymbol{\lambda}_h) \cdot \llbracket \underline{\mathbf{w}}_h \rrbracket_h = -w_h(\boldsymbol{\sigma}(\mathbf{u}), \underline{\mathbf{w}}_h) - \int_{\Omega} (\boldsymbol{\sigma}(\mathbf{u}) - \boldsymbol{\sigma}_h(\underline{\mathbf{u}}_h)) : \boldsymbol{\epsilon}_h(\underline{\mathbf{w}}_h) + \mu_1 \mathbb{S}_h(\underline{\mathbf{u}}_h, \underline{\mathbf{w}}_h) \\
& = -w_h(\boldsymbol{\sigma}(\mathbf{u}), \underline{\mathbf{w}}_h) - \int_{\Omega} (\boldsymbol{\sigma}(\mathbf{u}) - \boldsymbol{\sigma}_h(\mathbb{I}_h \mathbf{u})) : \boldsymbol{\epsilon}_h(\underline{\mathbf{w}}_h) + \mu_1 \mathbb{S}_h(\underline{\mathbf{u}}_h, \underline{\mathbf{w}}_h) \\
& \quad + \int_{\Omega} (\boldsymbol{\sigma}_h(\underline{\mathbf{u}}_h) - \boldsymbol{\sigma}_h(\mathbb{I}_h \mathbf{u})) : \boldsymbol{\epsilon}_h(\underline{\mathbf{w}}_h) \\
& \stackrel{(5.27)}{=} -w_h(\boldsymbol{\sigma}(\mathbf{u}), \underline{\mathbf{w}}_h) - \frac{E}{1+\nu} \int_{\Omega} (\boldsymbol{\epsilon}(\mathbf{u}) - \boldsymbol{\epsilon}_h(\mathbb{I}_h \mathbf{u})) : \boldsymbol{\epsilon}_h(\underline{\mathbf{w}}_h) + \mu_1 \mathbb{S}_h(\mathbb{I}_h \mathbf{u}, \underline{\mathbf{w}}_h) \\
& \quad + \int_{\Omega} (\boldsymbol{\sigma}_h(\underline{\mathbf{u}}_h) - \boldsymbol{\sigma}_h(\mathbb{I}_h \mathbf{u})) : \boldsymbol{\epsilon}_h(\underline{\mathbf{w}}_h) + \mu_1 \mathbb{S}_h(\underline{\mathbf{u}}_h - \mathbb{I}_h \mathbf{u}, \underline{\mathbf{w}}_h) \\
& \stackrel{(3.7), (5.25)}{\lesssim} -w_h(\boldsymbol{\sigma}(\mathbf{u}), \underline{\mathbf{w}}_h) + \mu_2 \|\nabla \mathbf{u} - \mathbb{G}_h^1 \mathbb{I}_h \mathbf{u}\|_{L^2(\Omega)} \|\underline{\mathbf{w}}_h\|_{1,h} \\
& \quad + \mu_2 \mathbb{S}_h(\mathbb{I}_h \mathbf{u}, \mathbb{I}_h \mathbf{u})^{\frac{1}{2}} \|\underline{\mathbf{w}}_h\|_{1,h} + \sqrt{\mu_2} \left(1 + \left(\frac{\nu}{1-2\nu}\right)^{\frac{1}{2}}\right) \|\underline{\mathbf{u}}_h - \mathbb{I}_h \mathbf{u}\|_{\text{en},h} \|\underline{\mathbf{w}}_h\|_{1,h} \\
& \quad + \mu_1 \mathbb{S}_h(\underline{\mathbf{u}}_h - \mathbb{I}_h \mathbf{u}, \underline{\mathbf{u}}_h - \mathbb{I}_h \mathbf{u})^{\frac{1}{2}} \|\underline{\mathbf{w}}_h\|_{1,h} \\
& \stackrel{(3.9)}{\lesssim} -w_h(\boldsymbol{\sigma}(\mathbf{u}), \underline{\mathbf{w}}_h) + \|\underline{\mathbf{w}}_h\|_{1,h} \left[\mu_2 \|\nabla \mathbf{u} - \mathbb{G}_h^1 \mathbb{I}_h \mathbf{u}\|_{L^2(\Omega)} \right. \\
& \quad \left. + \sqrt{\mu_2} \left(1 + \left(\frac{\nu}{1-2\nu}\right)^{\frac{1}{2}}\right) \|\underline{\mathbf{u}}_h - \mathbb{I}_h \mathbf{u}\|_{\text{en},h} + \sqrt{\mu_2} \|\underline{\mathbf{u}}_h - \mathbb{I}_h \mathbf{u}\|_{\text{en},h} + \mu_2 \mathbb{S}_h(\mathbb{I}_h \mathbf{u}, \mathbb{I}_h \mathbf{u})^{\frac{1}{2}} \right],
\end{aligned}$$

where we have used $\mu_1 \leq \mu_2$, $\frac{E}{1+\nu} \leq \mu_2$ and, to pass to the second line, we have introduced $\pm \boldsymbol{\sigma}_h(\mathbb{I}_h \mathbf{u}) : \boldsymbol{\epsilon}_h(\underline{\mathbf{w}}_h)$ in the second term of the first right-hand side. Using the discrete inf-sup condition (3.12) and the definitions (4.8) of $\boldsymbol{\mathcal{C}}_h$ and (4.9) of $\boldsymbol{\mathcal{W}}_h$, we infer

$$\|\Pi_{\mathcal{F}_T}^0 \boldsymbol{\lambda} - \boldsymbol{\lambda}_h\|_{-1/2, \Gamma} \lesssim \boldsymbol{\mathcal{W}}_h(\boldsymbol{\sigma}(\mathbf{u})) + \mu_2 \boldsymbol{\mathcal{C}}_h(\mathbf{u}, \mathbb{I}_h \mathbf{u}) + \sqrt{\mu_2} \left(1 + \left(\frac{\nu}{1-2\nu}\right)^{\frac{1}{2}}\right) \|\underline{\mathbf{u}}_h - \mathbb{I}_h \mathbf{u}\|_{\text{en},h}. \quad (5.31)$$

The bound (4.11) follows from the triangle inequality and (5.31), which concludes the lemma. \square

5.4 Proof of the error bound

In this section, we derive explicit bounds for the adjoint consistency in Lemma 5.7, the primal consistency in Lemma 5.8, and two results on product of higher-order variations of the Lagrange multiplier and the displacement (Lemma 5.9 and 5.10). Finally, we use these lemmas to prove the error estimates of Theorem 4.3.

Lemma 5.7 (Adjoint Consistency). *Recalling the definition (4.9) of the adjoint consistency error $\boldsymbol{\mathcal{W}}_h$, it holds that for all $\boldsymbol{\chi} \in \boldsymbol{\Sigma} \cap H^s(\mathcal{M})^{3 \times 3}$ for some $s \in (\frac{1}{2}, \frac{3}{2})$,*

$$\boldsymbol{\mathcal{W}}_h(\boldsymbol{\chi}) \lesssim h^s \left(|\boldsymbol{\chi}|_{H^s(\mathcal{M})} + |\gamma_n^+ \boldsymbol{\chi}|_{H^{s-\frac{1}{2}}(\Gamma)} \right).$$

Proof. Let $\mathbf{v}_h \in \mathbf{X}_{\text{grad},h,0}$, $\boldsymbol{\chi} \in \boldsymbol{\Sigma}$ and $\boldsymbol{\chi} \in H^s(\mathcal{M})^{3 \times 3}$, where $s \in (\frac{1}{2}, \frac{3}{2})$. Since $\boldsymbol{\chi}$ is symmetric, we have $\boldsymbol{\chi} : \boldsymbol{\epsilon}_h(\mathbf{v}_h) = \boldsymbol{\chi} : \mathbb{G}_h^1(\mathbf{v}_h)$ and thus, by (4.9),

$$\begin{aligned}
w_h(\boldsymbol{\chi}, \mathbf{v}_h) &= - \sum_{K \in \mathcal{M}} \int_K \boldsymbol{\Pi}_K^1 \boldsymbol{\chi} : \mathbb{G}_K^1(\mathbf{v}_h) + \int_{\Gamma} \Pi_{\mathcal{F}_\Gamma}^0(\gamma_n^+ \boldsymbol{\chi}) \cdot \llbracket \mathbf{v}_h \rrbracket_h - \sum_{K \in \mathcal{M}} \int_K \mathbf{v}_K \cdot \text{div } \boldsymbol{\chi} \\
&\stackrel{(3.3),(3.2)}{=} \sum_{K \in \mathcal{M}} \int_K \mathbf{v}_K \cdot \text{div}(\boldsymbol{\Pi}_K^1 \boldsymbol{\chi}) - \sum_{K \in \mathcal{M}} \sum_{\sigma \in \mathcal{F}_K} \int_{\sigma} \Upsilon_{K\sigma}^2 \mathbf{v}_h \cdot \boldsymbol{\Pi}_K^1 \boldsymbol{\chi} \mathbf{n}_{K\sigma} \\
&\quad + \sum_{\sigma \in \mathcal{F}_\Gamma} \int_{\sigma=K|L} \Pi_{\sigma}^0(\boldsymbol{\chi} \mathbf{n}_{K\sigma}) \cdot (\Upsilon_{K\sigma}^2 \mathbf{v}_h - \Upsilon_{L\sigma}^2 \mathbf{v}_h) - \sum_{K \in \mathcal{M}} \int_K \mathbf{v}_K \cdot \text{div } \boldsymbol{\chi} \\
&\stackrel{\text{IBP}}{=} - \sum_{K \in \mathcal{M}} \sum_{\sigma \in \mathcal{F}_K} \int_{\sigma} \mathbf{v}_K \cdot (\boldsymbol{\chi}|_K - \boldsymbol{\Pi}_K^1 \boldsymbol{\chi}) \mathbf{n}_{K\sigma} - \sum_{K \in \mathcal{M}} \sum_{\sigma \in \mathcal{F}_K} \int_{\sigma} \Upsilon_{K\sigma}^2 \mathbf{v}_h \cdot \boldsymbol{\Pi}_K^1 \boldsymbol{\chi} \mathbf{n}_{K\sigma} \\
&\quad + \sum_{K \in \mathcal{M}} \sum_{\sigma \in \mathcal{F}_K \cap \mathcal{F}_\Gamma} \int_{\sigma} \Upsilon_{K\sigma}^2 \mathbf{v}_h \cdot \Pi_{\sigma}^0(\boldsymbol{\chi} \mathbf{n}_{K\sigma}), \tag{5.32}
\end{aligned}$$

where the introduction of $\boldsymbol{\Pi}_K^1$ in the first line is justified by $\mathbb{G}_K^1(\mathbf{v}_h) \in \mathbb{P}^1(K)^{3 \times 3}$ and we recall that, for all $\sigma \in \mathcal{F}_\Gamma$, we have denoted by K and L the cells that contain σ and are, respectively, on the positive and negative side of Γ . Since $\Upsilon_{K\sigma}^2 \mathbf{v}_h = \Upsilon_{L\sigma}^2 \mathbf{v}_h$ for all $\sigma = K|L \in \mathcal{F}^{\text{int}} \setminus \mathcal{F}_\Gamma$, $\Upsilon_{K\sigma}^2 \mathbf{v}_h = 0$ for all $\sigma \in \mathcal{F}_K \cap \mathcal{F}^{\text{ext}}$, and the normal traces of $\boldsymbol{\chi}$ are continuous across Γ , we have

$$\begin{aligned}
\sum_{K \in \mathcal{M}} \sum_{\sigma \in \mathcal{F}_K} \int_{\sigma} \Upsilon_{K\sigma}^2 \mathbf{v}_h \cdot \boldsymbol{\chi} \mathbf{n}_{K\sigma} &= \sum_{K \in \mathcal{M}} \sum_{\sigma \in \mathcal{F}_K \cap \mathcal{F}_\Gamma} \int_{\sigma} \Upsilon_{K\sigma}^2 \mathbf{v}_h \cdot \boldsymbol{\chi} \mathbf{n}_{K\sigma} \\
&\quad + \underbrace{\sum_{K \in \mathcal{M}} \sum_{\sigma \in \mathcal{F}_K \setminus \mathcal{F}_\Gamma} \int_{\sigma} \Upsilon_{K\sigma}^2 \mathbf{v}_h \cdot \boldsymbol{\chi} \mathbf{n}_{K\sigma}}_{=0}. \tag{5.33}
\end{aligned}$$

Introducing $\pm \sum_{K \in \mathcal{M}} \sum_{\sigma \in \mathcal{F}_K} \int_{\sigma} \Upsilon_{K\sigma}^2 \mathbf{v}_h \cdot \boldsymbol{\chi} \mathbf{n}_{K\sigma}$ in (5.32) and invoking (5.33), we obtain

$$\begin{aligned}
w_h(\boldsymbol{\chi}, \mathbf{v}_h) &= - \sum_{K \in \mathcal{M}} \sum_{\sigma \in \mathcal{F}_K} \int_{\sigma} \mathbf{v}_K \cdot (\boldsymbol{\chi}|_K - \boldsymbol{\Pi}_K^1 \boldsymbol{\chi}) \mathbf{n}_{K\sigma} + \sum_{K \in \mathcal{M}} \sum_{\sigma \in \mathcal{F}_K} \int_{\sigma} \Upsilon_{K\sigma}^2 \mathbf{v}_h \cdot (\boldsymbol{\chi}|_K - \boldsymbol{\Pi}_K^1 \boldsymbol{\chi}) \mathbf{n}_{K\sigma} \\
&\quad + \sum_{K \in \mathcal{M}} \sum_{\sigma \in \mathcal{F}_K \cap \mathcal{F}_\Gamma} \int_{\sigma} \Upsilon_{K\sigma}^2 \mathbf{v}_h \cdot (\Pi_{\sigma}^0(\boldsymbol{\chi} \mathbf{n}_{K\sigma}) - \boldsymbol{\chi} \mathbf{n}_{K\sigma}) \\
&= \underbrace{\sum_{K \in \mathcal{M}} \sum_{\sigma \in \mathcal{F}_K} \int_{\sigma} (\Upsilon_{K\sigma}^2 \mathbf{v}_h - \mathbf{v}_K) \cdot (\boldsymbol{\chi}|_K - \boldsymbol{\Pi}_K^1 \boldsymbol{\chi}) \mathbf{n}_{K\sigma}}_{I_1} \\
&\quad + \underbrace{\sum_{K \in \mathcal{M}} \sum_{\sigma \in \mathcal{F}_K \cap \mathcal{F}_\Gamma} \int_{\sigma} (\Upsilon_{K\sigma}^2 \mathbf{v}_h - \Pi_{\sigma}^0 \Upsilon_{K\sigma}^2 \mathbf{v}_h) \cdot (\Pi_{\sigma}^0(\boldsymbol{\chi} \mathbf{n}_{K\sigma}) - \boldsymbol{\chi} \mathbf{n}_{K\sigma})}_{I_2}. \tag{5.34}
\end{aligned}$$

Note that the introduction of $\Pi_{\sigma}^0 \Upsilon_{K\sigma}^2 \mathbf{v}_h$ in I_2 is justified by the definition of the orthogonal projector, which gives $\int_{\sigma} \Pi_{\sigma}^0 \Upsilon_{K\sigma}^2 \mathbf{v}_h \cdot (\Pi_{\sigma}^0(\boldsymbol{\chi} \mathbf{n}_{K\sigma}) - \boldsymbol{\chi} \mathbf{n}_{K\sigma}) = 0$. Using the Cauchy-Schwarz inequality, the fractional multiplicative trace inequality [27, Remark 2.6], and the approximation properties of $\boldsymbol{\Pi}_K^1$ and Π_{σ}^0 , obtained by interpolating the estimates of [25, Theorem 1.45] for integral Sobolev exponents and the mesh regularity assumption, we obtain

$$I_1 \lesssim \sum_{K \in \mathcal{M}} \left(\sum_{\sigma \in \mathcal{F}_K} \|\mathbf{v}_K - \Upsilon_{K\sigma}^2 \mathbf{v}_h\|_{L^2(\sigma)} \right)$$

$$\begin{aligned}
& \times \left(h_K^{-\frac{1}{2}} \|\boldsymbol{\chi} - \boldsymbol{\Pi}_K^1 \boldsymbol{\chi}\|_{L^2(K)} + h_K^{\min(s-\frac{1}{2}, \frac{1}{2})} |\boldsymbol{\chi} - \boldsymbol{\Pi}_K^1 \boldsymbol{\chi}|_{H^{\min(s,1)}(K)} \right) \\
& \lesssim \sum_{K \in \mathcal{M}} \sum_{\sigma \in \mathcal{F}_K} h_K^{-\frac{1}{2}} \|\mathbf{v}_K - \Upsilon_{K\sigma}^2 \mathbf{v}_h\|_{L^2(\sigma)} h_K^s |\boldsymbol{\chi}|_{H^s(K)} \\
& \lesssim \left(\sum_{K \in \mathcal{M}} h_K^{2s} |\boldsymbol{\chi}|_{H^s(K)}^2 \right)^{1/2} \left(\sum_{K \in \mathcal{M}} \left(\sum_{\sigma \in \mathcal{F}_K} h_K^{-\frac{1}{2}} \|\mathbf{v}_K - \Upsilon_{K\sigma}^2 \mathbf{v}_h\|_{L^2(\sigma)} \right)^2 \right)^{1/2} \\
& \stackrel{(5.3)}{\lesssim} h^s |\boldsymbol{\chi}|_{H^s(\mathcal{M})} \left(\sum_{K \in \mathcal{M}} \|\mathbf{v}_h\|_{1,K}^2 \right)^{1/2},
\end{aligned}$$

and

$$\begin{aligned}
I_2 & \lesssim \sum_{K \in \mathcal{M}} \sum_{\sigma \in \mathcal{F}_K \cap \mathcal{F}_\Gamma} h_\sigma \|\nabla_\sigma \Upsilon_{K\sigma}^2 \mathbf{v}_h\|_{L^2(\sigma)} h_\sigma^{s-\frac{1}{2}} |\gamma_{\mathbf{n}}^+ \boldsymbol{\chi}|_{H^{s-\frac{1}{2}}(\sigma)} \\
& \lesssim \left(\sum_{K \in \mathcal{M}} \sum_{\sigma \in \mathcal{F}_K \cap \mathcal{F}_\Gamma} h_\sigma \|\nabla_\sigma \Upsilon_{K\sigma}^2 \mathbf{v}_h\|_{L^2(\sigma)}^2 \right)^{1/2} \left(\sum_{K \in \mathcal{M}} \sum_{\sigma \in \mathcal{F}_K \cap \mathcal{F}_\Gamma} h_\sigma^{2s} |\gamma_{\mathbf{n}}^+ \boldsymbol{\chi}|_{H^{s-\frac{1}{2}}(\sigma)}^2 \right)^{1/2} \\
& \stackrel{(5.2)}{\lesssim} h^s |\gamma_{\mathbf{n}}^+ \boldsymbol{\chi}|_{H^{s-\frac{1}{2}}(\Gamma)} \left(\sum_{K \in \mathcal{M}} \|\mathbf{v}_h\|_{1,K}^2 \right)^{1/2}.
\end{aligned}$$

Substituting bounds of I_1 and I_2 in (5.34) and using (4.9) concludes the lemma. \square

Lemma 5.8. *Let $\mathbf{u} \in H_0^1(\Omega \setminus \bar{\Gamma})^3 \cap H^{\frac{3}{2}+\tau}(\mathcal{M})^3$ with $0 < \tau \leq 1$. Then, the following estimate holds:*

$$\mathfrak{E}_h(\mathbf{u}, \mathbb{I}_h \mathbf{u}) \lesssim h^{\frac{1}{2}+\tau} |\mathbf{u}|_{H^{\frac{3}{2}+\tau}(\mathcal{M})}. \quad (5.35)$$

Proof. We first note that the regularity assumption ensures that $\mathbf{u} \in C_0^0(\bar{\Omega} \setminus \Gamma)^3$. Let $K \in \mathcal{M}$ and \mathbf{q} be the $L^2(K)$ -orthogonal projection of \mathbf{u} on $\mathbb{P}^1(K)^3$. By the approximation properties of the polynomial projector [25, Theorem 1.45] we have

$$|\mathbf{u} - \mathbf{q}|_{H^s(K)} \lesssim h^{\frac{3}{2}+\tau-s} |\mathbf{u}|_{H^{\frac{3}{2}+\tau}(K)}, \quad \forall s \in \left[0, \frac{3}{2} + \tau\right]. \quad (5.36)$$

Applying the bound [25, Eq.(5.110)] to $\mathbf{u} - \mathbf{q}$ yields

$$\max_K |\mathbf{u} - \mathbf{q}| \lesssim h_K^\tau |\mathbf{u}|_{H^{\frac{3}{2}+\tau}(K)}. \quad (5.37)$$

Now, let us gather the degrees of freedom on K of $\mathbb{I}_h \mathbf{u} - \mathbb{I}_h \mathbf{q}$.

$$\begin{aligned}
|(\mathbb{I}_h \mathbf{u} - \mathbb{I}_h \mathbf{q})_{\mathcal{K}_s}| & = |(\mathbf{u} - \mathbf{q})(\mathbf{x}_s)| \leq \max_K |\mathbf{u} - \mathbf{q}|, \quad \forall s \in \mathcal{V}_K, \\
|(\mathbb{I}_h \mathbf{u} - \mathbb{I}_h \mathbf{q})_{\mathcal{K}_e}| & = |\Pi_e^0((\mathbf{u} - \mathbf{q})|_K)| \leq \max_K |\mathbf{u} - \mathbf{q}|, \quad \forall e \in \mathcal{E}_K, \\
|(\mathbb{I}_h \mathbf{u} - \mathbb{I}_h \mathbf{q})_{\mathcal{K}_\sigma}| & = |\Pi_\sigma^0((\mathbf{u} - \mathbf{q})|_K)| \leq \max_K |\mathbf{u} - \mathbf{q}|, \quad \forall \sigma \in \mathcal{F}_K, \\
|(\mathbb{I}_h \mathbf{u} - \mathbb{I}_h \mathbf{q})_K| & = |\Pi_K^0(\mathbf{u} - \mathbf{q}) + (\tilde{\mathbf{u}}_K - \tilde{\mathbf{q}}_K)| \leq \max_K |\mathbf{u} - \mathbf{q}| + |\tilde{\mathbf{u}}_K|,
\end{aligned} \quad (5.38)$$

where, in the last relation, we have used $\tilde{\mathbf{q}}_K = 0$ in virtue of the argument in Remark 4.1. Let $f \in \mathbb{P}^1(K)$ be such that $\int_K f = 0$ and $\tilde{\mathbf{u}}_K = \nabla f$. Since $\Pi_K^0 f = 0$, by (4.2),

$$\begin{aligned} \|\tilde{\mathbf{u}}_K\|_{L^2(K)}^2 &\leq \sum_{\sigma \in \mathcal{F}_K} \|\mathbf{u}|_K - \Upsilon_{K\sigma}^2 \mathbb{I}_h \mathbf{u}\|_{L^2(\sigma)} \|f\|_{L^2(\sigma)} \\ &\leq \sum_{\sigma \in \mathcal{F}_K} \|\mathbf{u}|_K - \Upsilon_{K\sigma}^2 \mathbb{I}_h \mathbf{u}\|_{L^2(\sigma)} \|f - \Pi_K^0 f\|_{L^2(\sigma)} \\ &\leq \sum_{\sigma \in \mathcal{F}_K} h_\sigma \|\mathbf{u}|_K - \Upsilon_{K\sigma}^2 \mathbb{I}_h \mathbf{u}\|_{L^\infty(\sigma)} h_K^{1/2} \|\nabla f\|_{L^2(K)} \end{aligned}$$

where we have used the trace approximation properties of Π_K^0 . Simplify by $\|\nabla f\|_{L^2(K)} = \|\tilde{\mathbf{u}}_K\|_{L^2(K)}$ and use (4.7) to introduce $\mathbf{q} - \Upsilon_{K\sigma}^2 \mathbb{I}_h \mathbf{q} = 0$:

$$\|\tilde{\mathbf{u}}_K\|_{L^2(K)} \leq h_K^{3/2} \sum_{\sigma \in \mathcal{F}_K} \|(\mathbf{u} - \mathbf{q})|_K - \Upsilon_{K\sigma}^2 \mathbb{I}_h (\mathbf{u} - \mathbf{q})\|_{L^\infty(\sigma)}.$$

Then, we invoke [21, (A.10)] to get $\|\Upsilon_{K\sigma}^2 \mathbb{I}_h (\mathbf{u} - \mathbf{q})\|_{L^\infty(\sigma)} \lesssim \max_{\bar{\sigma}} |\mathbf{u}|_K - \mathbf{q}| \leq \max_{\bar{K}} |\mathbf{u} - \mathbf{q}|$, which allows us to conclude

$$|\tilde{\mathbf{u}}_K| \lesssim \max_{\bar{K}} |\mathbf{u} - \mathbf{q}|. \quad (5.39)$$

Using Lemma 5.2 and (5.38)–(5.39), it follows that

$$\begin{aligned} \left(\|\mathbb{G}_K^1 \mathbb{I}_h (\mathbf{u} - \mathbf{q})\|_{L^2(K)}^2 + \mathbb{S}_K (\mathbb{I}_h \mathbf{u} - \mathbb{I}_h \mathbf{q}, \mathbb{I}_h \mathbf{u} - \mathbb{I}_h \mathbf{q}) \right)^{1/2} &= \|\mathbb{I}_h \mathbf{u} - \mathbb{I}_h \mathbf{q}\|_{1,K} \\ &\lesssim h_K^{1/2} \max_{\bar{K}} |\mathbf{u} - \mathbf{q}| \stackrel{(5.37)}{\lesssim} h_K^{\frac{1}{2} + \tau} |\mathbf{u}|_{H^{\frac{3}{2} + \tau}(K)}. \end{aligned}$$

Using (4.5) and (5.19) in the above inequality, we get

$$\left(\|\mathbb{G}_K^1 \mathbb{I}_h \mathbf{u} - \nabla \mathbf{q}\|_{L^2(K)}^2 + \mathbb{S}_K (\mathbb{I}_h \mathbf{u}, \mathbb{I}_h \mathbf{u}) \right)^{1/2} \lesssim h_K^{\frac{1}{2} + \tau} |\mathbf{u}|_{H^{\frac{3}{2} + \tau}(K)}.$$

Recalling the definition (4.8) of \mathfrak{C}_h , the estimate (5.35) follows by introducing $\pm \nabla \mathbf{u}$ in the left-hand side above, using a triangle inequality, the approximation property (5.36) (with $s = 1$), squaring, summing over K , using the bound $h_K \leq h$ and taking the square root. \square

Lemma 5.9. *Let $(\mathbf{u}, \boldsymbol{\lambda})$ be the solution of (2.2), and assume that $\mathbf{u} \in H_0^1(\Omega \setminus \bar{\Gamma})^3 \cap H^{\frac{3}{2} + \tau}(\mathcal{M})^3$ with $0 < \tau \leq 1$ and $\sigma \in \mathcal{F}_\Gamma$. Then, the following estimate holds:*

$$\int_{\sigma} (\lambda_{\mathbf{n}} - \Pi_{\sigma}^0 \lambda_{\mathbf{n}}) (\llbracket \mathbf{u} \rrbracket_{\mathbf{n}} - \Pi_{\sigma}^0 \llbracket \mathbf{u} \rrbracket_{\mathbf{n}}) \lesssim h_{\sigma}^{1+2\tau} (|\lambda_{\mathbf{n}}|_{H^{\tau}(\sigma)}^2 + |\nabla \llbracket \mathbf{u} \rrbracket_{\mathbf{n}}|_{H^{\tau}(\sigma)}^2). \quad (5.40)$$

Proof. Let $\Gamma_{C\sigma} := \{x \in \sigma : \llbracket \mathbf{u}(x) \rrbracket_{\mathbf{n}} = \mathbf{0}\}$ and $\Gamma_{N\sigma} := \{x \in \Gamma : \llbracket \mathbf{u}(x) \rrbracket_{\mathbf{n}} < \mathbf{0}\}$ be the contact and non-contact zones on σ . If $|\Gamma_{N\sigma}| > 0$ and $|\Gamma_{C\sigma}| > 0$ then the arguments leading to [33, Eq. (33) and (34)] show that (5.40) hold with $h_{\sigma}^{1+2\tau}$ replaced by either $\frac{h_{\sigma}^{2(1+\tau)}}{|\Gamma_{N\sigma}|^{1/2}}$ or $\frac{h_{\sigma}^{2(1+\tau)}}{|\Gamma_{C\sigma}|^{1/2}}$. Since $\sigma = \Gamma_{N\sigma} \sqcup \Gamma_{C\sigma}$, one of $|\Gamma_{N\sigma}|$ or $|\Gamma_{C\sigma}|$ is larger than $|\sigma|/2 \gtrsim h_{\sigma}^2$ (by mesh regularity assumption); picking the estimate corresponding to that largest set yields (5.40).

If one of $|\Gamma_{N\sigma}|$ and $|\Gamma_{C\sigma}|$ vanishes, say $|\Gamma_{C\sigma}| = 0$ to fix the ideas, then by complementarity condition we have $\lambda_{\mathbf{n}} = 0$ on σ , so $\Pi_{\sigma}^0 \lambda_{\mathbf{n}} = 0$ and thus the left-hand side of (5.40) vanishes, making this inequality trivial. \square

Lemma 5.10. *Let $(\mathbf{u}, \boldsymbol{\lambda})$ be the solution of (2.2), and consider real parameters \mathbf{r} , $s_{\mathbf{r}}$ and $t_{\mathbf{r}}$ as in Theorem 4.3. Then,*

$$\int_{\Gamma} (\boldsymbol{\lambda} - \Pi_{\mathcal{F}_\Gamma}^0 \boldsymbol{\lambda}) \cdot ([\![\mathbf{u}]\!] - \Pi_{\mathcal{F}_\Gamma}^0 [\![\mathbf{u}]\!]) \lesssim h^{1+2\mathbf{r}} (|\boldsymbol{\lambda}|_{H^{s_{\mathbf{r}}}(\mathcal{F}_\Gamma)}^2 + \|[\![\mathbf{u}]\!]\|_{H^{t_{\mathbf{r}}}(\mathcal{F}_\Gamma)}^2). \quad (5.41)$$

Proof. In case of frictionless contact ($g = 0$), we have

$$\int_{\sigma} (\boldsymbol{\lambda} - \Pi_{\sigma}^0 \boldsymbol{\lambda}) \cdot ([\![\mathbf{u}]\!] - \Pi_{\sigma}^0 [\![\mathbf{u}]\!]) = \int_{\sigma} (\lambda_{\mathbf{n}} - \Pi_{\sigma}^0 \lambda_{\mathbf{n}}) ([\![\mathbf{u}]\!]_{\mathbf{n}} - \Pi_{\sigma}^0 [\![\mathbf{u}]\!]_{\mathbf{n}}) \quad \forall \sigma \in \mathcal{F}_\Gamma.$$

By Lemma 5.9 and since $t_{\mathbf{r}} = 1 + \mathbf{r}$ (as $g = 0$), we infer

$$\int_{\sigma} (\boldsymbol{\lambda} - \Pi_{\sigma}^0 \boldsymbol{\lambda}) \cdot ([\![\mathbf{u}]\!] - \Pi_{\sigma}^0 [\![\mathbf{u}]\!]) \lesssim h^{1+2\mathbf{r}} (|\boldsymbol{\lambda}|_{H^{\mathbf{r}}(\sigma)}^2 + \|[\![\mathbf{u}]\!]\|_{H^{t_{\mathbf{r}}}(\sigma)}^2) \quad \forall \sigma \in \mathcal{F}_\Gamma.$$

Adding over all the faces of \mathcal{F}_Γ yields (5.41).

In the case with friction, i.e., $g \neq 0$, the estimate follows directly from the Cauchy-Schwarz inequality, approximation properties of the projection operator $\Pi_{\mathcal{F}_\Gamma}^0$ [25, Theorem 1.45], and Young's inequality (note that this simple approach is only possible because of the restriction $0 \leq \mathbf{r} \leq 1/2$, instead of the larger range $0 \leq \mathbf{r} < 1$ allowed by the finer estimate obtained above when $g = 0$). \square

Proof of Theorem 4.3: From Theorem 4.2, Lemma 5.7, Lemma 5.8 and Lemma 5.10, we obtain

$$\begin{aligned} \|\underline{\mathbf{u}}_h - \mathbb{I}_h \mathbf{u}\|_{\text{en},h} &\lesssim h^{\frac{1}{2}+\mathbf{r}} \left[\frac{1}{\sqrt{\mu_1}} \left(|\boldsymbol{\sigma}(\mathbf{u})|_{H^{\frac{1}{2}+\mathbf{r}}(\mathcal{M})} + |\boldsymbol{\lambda}|_{H^{\mathbf{r}}(\Gamma)} \right) + \sqrt{\mu_2} |\mathbf{u}|_{H^{\frac{3}{2}+\mathbf{r}}(\mathcal{M})} \right. \\ &\quad \left. + |\boldsymbol{\lambda}|_{H^{s_{\mathbf{r}}}(\mathcal{F}_\Gamma)} + \|[\![\mathbf{u}]\!]\|_{H^{t_{\mathbf{r}}}(\mathcal{F}_\Gamma)} \right]. \end{aligned}$$

This completes the bound of (4.12). Finally, the bound (4.13) is obtained from (4.11), Lemmas 5.6–5.8, and the approximation property [25, Theorem 1.45] of $\Pi_{\mathcal{F}_\Gamma}^0$. This concludes the theorem. \square

6 Numerical Experiments

In this section, we assess the numerical convergence of the proposed discretisation for the poromechanical model with frictional contact at matrix–fracture interfaces. The first and second Lamé coefficients are related to Young's modulus E and Poisson's ratio ν by $G := \frac{E}{2(1+\nu)}$, $L := \frac{\nu E}{(1+\nu)(1-2\nu)}$, respectively.

The subsequent sections present a series of test cases. Sections 6.1–6.3 employ the same families of meshes having uniform Cartesian, tetrahedral, and hexahedral cells. Section 6.1 analyzes the convergence of the frictionless formulation using a 3D manufactured analytical solution with a single fracture. Section 6.2 focuses on a 3D configuration governed by the Tresca friction law, while Section 6.3 examines the performance of the method in nearly incompressible regimes for Lamé coefficient $L \in \{1, 10^4, 10^6\}$. Finally, Section 6.4 turns to a more challenging 3D Discrete Fracture–Matrix (DFM) model without an analytical solution, relying on tetrahedral meshes refined along the fracture network.

In all the following experiments, the fracture face-wise Lagrange multiplier enables the reformulation of the variational inequality (3.5b), together with the constraint $\lambda_h \in \mathcal{C}_{f,h}$, into a system of nonlinear equations. These equations involve the projection operators $[r]_+ = \max(0, r)$ and $[\xi]_g = \text{projection of } \xi \in \mathbb{R}^3 \text{ onto the ball centered at 0 with radius } g$, and are written

$$\begin{cases} \lambda_{h,\mathbf{n}} := [\lambda_{h,\mathbf{n}} + \beta_{h,\mathbf{n}} \llbracket \mathbf{u}_h \rrbracket_{h,\mathbf{n}}]_+, \\ \lambda_{h,\tau} := [\lambda_{h,\tau} + \beta_{h,\tau} \llbracket \mathbf{u}_h \rrbracket_{h,\tau}]_g, \end{cases}$$

where $\beta_{h,\mathbf{n}} > 0$, and $\beta_{h,\tau} > 0$ are face-wise constant quantities defined along Γ . The resulting nonlinear system is solved with a semi-smooth Newton algorithm. The stopping criteria is set to 10^{-12} on the relative residual, and the linear system at each iteration is solved using the Pardiso LU solver.

6.1 3D manufactured solution for a frictionless contact ($g = 0$) mechanical model

Following [31], we consider the 3D domain $\Omega = (-1, 1)^3$ with a single non-immersed fracture $\Gamma = \{0\} \times (-1, 1)^2$. The friction coefficient g is set to zero, corresponding to frictionless contact, and the Lamé coefficients are set to be $G = L = 1$. The exact solution is defined by

$$\mathbf{u}(x, y, z) = \begin{cases} \begin{pmatrix} q(x, y)p(z) \\ p(z) \\ x^2p(z) \end{pmatrix} & \text{if } z \geq 0, \\ \begin{pmatrix} h(x)p^+(z) \\ h(x)(p^+(z))' \\ -\int_0^x h(\xi) d\xi (p^+(z))' \end{pmatrix} & \text{if } z < 0, x < 0, \\ \begin{pmatrix} h(x)p^-(z) \\ h(x)(p^-(z))' \\ -\int_0^x h(\xi) d\xi (p^-(z))' \end{pmatrix} & \text{if } z < 0, x \geq 0. \end{cases}$$

with $q(x, y) = -\sin(\frac{\pi x}{2}) \cos(\frac{\pi y}{2})$, $p(z) = z^2$, $h(x) = \cos(\frac{\pi x}{2})$, $p^+(z) = z^4$, and $p^-(z) = 2z^4$. The function \mathbf{u} is designed to satisfy the frictionless contact conditions at the matrix-fracture interface Γ . The right-hand side is $\mathbf{f} = -\text{div } \boldsymbol{\sigma}(\mathbf{u})$ and the Dirichlet boundary conditions on $\partial\Omega$ are deduced from \mathbf{u} . Note that the fracture Γ is in contact state for $z > 0$ ($\llbracket \mathbf{u} \rrbracket_{\mathbf{n}} = 0$) and open for $z < 0$, with a normal jump $\llbracket \mathbf{u} \rrbracket_{\mathbf{n}} = -\min(z, 0)^4$ depending only on z .

This numerical experiment is performed on families of uniform Cartesian, tetrahedral, and hexahedral meshes. Starting from uniform Cartesian meshes, the hexahedral families – hereafter called Hexa-cut are generated by random perturbations of the vertices (except those on the fracture) and by cutting non-planar faces into two triangles. We measure the L^2 -norms of $\mathbf{u} - \Upsilon_h^2(\mathbf{u}_h)$, $\llbracket \mathbf{u} \rrbracket - \llbracket \mathbf{u}_h \rrbracket_h$, $\nabla \mathbf{u} - \nabla \Upsilon_h^2(\mathbf{u}_h)$, and $\lambda_{\mathbf{n}} - \lambda_{h,\mathbf{n}}$ versus the cubic root of the number of cells. Corresponding to these errors, the convergence rates of the DDR scheme are illustrated in Figure 6.1. The results show that the convergence on the Lagrange multiplier is of order 1; this is coherent with the estimate (4.13) which predicts a rate of almost 3/2 in discrete $H^{-1/2}$ -like norm, and would naturally makes us expect a rate of almost 1 in L^2 -norm. For the displacement, (4.12)

predicts a rate slightly below $3/2$ in energy norm, which would translate into the same rate for the gradient; this is observed on tetrahedral and hexa-cut meshes, but Cartesian meshes seem to produce a super-convergence with a rate of almost 2. The approximation of the displacement and its jump seems to be higher than those for the energy norm, albeit not by a full order: all three meshes indicate an order 2 convergence on these measures. Moreover, Figure 6.3(a) compares the L^2 -norm of $\nabla \mathbf{u} - \nabla \Upsilon_h^2(\mathbf{u}_h)$ between the lowest-order method from [32] and the current higher order scheme on tetrahedral meshes. The comparison reveals that, to achieve a given degree of accuracy, the scheme presented here requires significantly fewer degrees of freedom than the method in [32], highlighting the improved efficiency of the higher-order formulation.

6.2 3D manufactured solution for the Tresca friction model

We consider the same domain, fracture and Lamé coefficients as in Section 6.1, but the Tresca threshold is now set at $g = 1$. Following [32], the exact solution is given by

$$\mathbf{u}(x, y, z) = \begin{cases} \begin{pmatrix} h(x, y)P(z) - gy \\ P(z) \\ x^2P(z) \end{pmatrix} & \text{if } z \geq 0, \\ \begin{pmatrix} h(x, y)Q(z) - gy \\ 2Q(z) \\ x^2Q(z) \end{pmatrix} & \text{if } z < 0, x < 0, \\ \begin{pmatrix} h(x, y)Q(z) - gy \\ Q(z) \\ x^2Q(z) \end{pmatrix} & \text{if } z < 0, x \geq 0, \end{cases}$$

with $h(x, y) = -\sin(x) \cos(y)$, $P(z) = z^2$, and $Q(z) = z^2/4$, and satisfies the Tresca frictional-contact conditions at the matrix–fracture interface Γ . The right-hand side $\mathbf{f} = -\operatorname{div} \boldsymbol{\sigma}(\mathbf{u})$ and the Dirichlet boundary conditions on $\partial\Omega$ are obtained from \mathbf{u} . The fracture Γ is in slippy-contact for $z < 0$ and sticky-contact for $z > 0$. The convergence of the scheme is investigated on the same families of meshes as before, with the results given in Figure 6.2. According to theoretical predictions, the displacement gradient $\nabla \mathbf{u}$ and the Lagrange multiplier $\lambda_{\mathbf{n}}$ should converge with order 1 (see Theorem 4.3 and remember that $g \neq 0$ here). The numerical results show that, on all three mesh families, the approximation of the gradient is much better, reaching orders close to 2. The Lagrange multiplier variable converges with order 1, which is slightly better than the expected rate of 0.5 ((4.13) predicts a rate of 1 in discrete $H^{-1/2}$ -norm, which would suggest a rate of 0.5 in L^2 -norm). Given that the improved convergence occurs for a range of unstructured meshes, we believe that the reason for the discrepancy between the theoretical results and the observed rates of convergence is to be found in limitations of the analysis when $g \neq 0$, and is not due to a specific behaviour of the scheme on these particular test cases. We note that, even for quadratic finite elements, we are not aware of an analysis for mixed formulations that proves an order > 1 convergence in energy norm for the Tresca model with friction (the study in [45] is carried out with $g = 0$). On the other hand, such a result is proved for the Finite Element and Hybrid High Order discretisations based on Nitsche’s formulation [15, 17].

For the displacement itself and its jump, we notice a rate of about 2 – which is somewhat expected since Theorem 4.3 predicts an order 1 for the gradient – and even larger than 2 on Cartesian meshes (this superconvergence is probably due to the symmetries of this particular mesh). Figure 6.3(b) demonstrates a similar efficiency gain for the higher order method over the lowest order case, consistent with the results from the test case in Section 6.1.

6.3 3D manufactured solution to test incompressibility for the Tresca friction model

The geometry and mesh are the same as in the previous test cases, but the Lamé coefficient are now $G = 1$, $L \in \{1, 10^4, 10^6\}$, and the Tresca threshold g is set to $1/L$. The exact solution is defined by

$$\mathbf{u}(x, y, z) = \begin{cases} \begin{pmatrix} x^3(\cos(y) + \sin(z)) \\ -3x^2 \sin(y) \\ 3x^2 \cos(z) \end{pmatrix} + \frac{1}{L} \begin{pmatrix} h(x, y)P(z) - y \\ P(z) \\ x^2P(z) \end{pmatrix} & \text{if } z \geq 0, \\ \begin{pmatrix} x^3(\cos(y) + \sin(z)) \\ -3x^2 \sin(y) \\ 3x^2 \cos(z) \end{pmatrix} + \frac{1}{L} \begin{pmatrix} h(x, y)Q(z) - y \\ 2Q(z) \\ x^2Q(z) \end{pmatrix} & \text{if } z < 0, x < 0, \\ \begin{pmatrix} x^3(\cos(y) + \sin(z)) \\ -3x^2 \sin(y) \\ 3x^2 \cos(z) \end{pmatrix} + \frac{1}{L} \begin{pmatrix} h(x, y)Q(z) - y \\ Q(z) \\ x^2Q(z) \end{pmatrix} & \text{if } z < 0, x \geq 0, \end{cases}$$

with $h(x, y) = -\sin(x) \cos(y)$, $P(z) = z^2$, and $Q(z) = z^2/4$, is designed to satisfy the Tresca frictional-contact conditions at the matrix–fracture interface Γ . The right-hand side $\mathbf{f} = -\operatorname{div} \boldsymbol{\sigma}(\mathbf{u})$ and the Dirichlet boundary conditions on $\partial\Omega$ are deduced from \mathbf{u} . As in section 6.2, we have that the fracture Γ is in slippy-contact for $z < 0$ and sticky-contact for $z > 0$. Convergence of the scheme is examined on a family of meshes, with the convergence rates for each value of L is reported in Table 6.1. As before we notice an order 2 convergence on the gradient but, more importantly, we see that the magnitude of the error remains the same no matter how high the second Lamé coefficient becomes. This demonstrate the fact that the scheme is locking-free in the quasi-incompressible limit, which is consistent with our error estimates (see Remark 4.3). We further investigates the conditioning of the method in the nearly incompressible regime. Keeping Young’s modulus $E = 1$, we vary the Poisson ratio ν towards 0.5 on the third tetrahedral mesh (with size $h = 6.75\text{e-}01$) and the third hexa-cut mesh (with size $h = 5.58\text{e-}01$). Figure 6.4 reports the condition number of the global stiffness matrix, and shows that it seems to grow almost linearly with respect to $1/(0.5 - \nu)$.

6.4 3D Discrete Fracture Matrix (DFM) model with intersecting fractures

We consider the three-dimensional domain $\Omega = (0, 1)^3$ that contains the fracture network depicted in Figure 6.5. The meshes are produced using **GMesh**, which provides tetrahedral meshes compliant with the fracture network [37]. The material is assumed to be isotropic and homogeneous with Young’s modulus $E = 4 \times 10^9$ and Poisson’s ratio $\nu = 0.2$, yielding a shear modulus $L = \frac{5}{3} \times 10^9$. The Tresca model governs the friction model with a constant friction coefficient $g = 4 \times 10^6$. Dirichlet boundary conditions are prescribed on the top and bottom surfaces: $\mathbf{u} = \mathbf{0}$ at $z = 0$ and $\mathbf{u} = [0.0015, -0.0015, -0.002]$ at $z = 1$. Homogeneous Neumann conditions are imposed on the lateral boundaries. In the numerical experiments, the normal and tangential penalty parameters are set to $\beta_{h,\mathbf{n}} = 10^6 = \beta_{h,\boldsymbol{\tau}}$. In practice, the nonlinear convergence is only weakly sensitive to the choice of the parameters $\beta_{h,\mathbf{n}}$ and $\beta_{h,\boldsymbol{\tau}}$, which are both taken as a small fraction, typically 10^{-3} , of the first Lamé coefficient $\frac{E}{1+\nu}$. A high degree of robustness of the nonlinear convergence is observed for values ranging from about $10^{-3} \frac{E}{1+\nu}$ to $\frac{E}{1+\nu}$. The natural scaling with respect to the mesh would be $1/h_\sigma$, where h_σ denotes the diameter of the face σ , but we have noted this scaling does not appear to be necessary in the simulations. For a numerical

Mesh Size	$L = 1$		$L = 10^4$		$L = 10^6$	
	E	Order	E	Order	E	Order
1.73e+00	1.73e-01	–	1.94e-01	–	1.94e-01	–
8.66e-01	4.55e-02	1.93	5.06e-02	1.94	5.06e-02	1.94
4.33e-01	1.07e-02	2.08	1.21e-02	2.06	1.21e-02	2.06
2.16e-01	2.63e-03	2.04	2.99e-03	2.02	2.99e-03	2.02
1.08e-01	6.53e-04	2.01	7.44e-04	2.01	7.44e-04	2.01

(a) Cartesian Mesh

Mesh Size	$L = 1$		$L = 10^4$		$L = 10^6$	
	E	Order	E	Order	E	Order
1.275e+00	6.42e-02	–	8.39e-02	–	8.40e-02	–
1.05e+00	2.89e-02	4.14	3.45e-02	4.61	3.45e-02	4.61
6.75e-01	1.61e-02	1.31	2.00e-02	1.23	2.00e-02	1.23
4.12e-01	5.48e-03	2.20	6.36e-03	2.33	6.36e-03	2.33
2.95e-01	2.97e-03	1.84	3.29e-03	1.98	3.29e-03	1.98

(b) Tetrahedral Mesh

Mesh Size	$L = 1$		$L = 10^4$		$L = 10^6$	
	E	Order	E	Order	E	Order
1.82e+00	2.08e-01	–	2.27e-01	–	2.27e-01	–
1.01e+00	6.48e-02	1.99	7.16e-02	1.97	7.16e-02	1.97
5.58e-01	1.65e-02	2.30	1.86e-02	2.26	1.86e-02	2.26
2.86e-01	4.34e-03	2.01	4.86e-03	2.02	4.86e-03	2.02
1.45e-01	1.14e-03	1.98	1.24e-03	2.02	1.24e-03	2.02

(c) Hexa-cut Mesh

Table 6.1: Order of convergence of $E = \|\nabla \mathbf{u} - \nabla \Upsilon_h^2(\underline{\mathbf{u}}_h)\|_{L^2(\mathcal{T}_h)}$ with different values of L for different mesh types. Test case of Section 6.3.

investigation of the sensitivity of the nonlinear convergence to the choice of these parameters, we refer to [9].

In this study, we focus on the qualitative behavior of the solution. Figure 6.6(a) displays the computed contact state, while Figure 6.6(b) displays the normal component of the displacement jump across the fracture network. The superior performance of the higher-order scheme is demonstrated in Figure 6.9 by the mean of the normal component of the discrete Lagrange multiplier $\lambda_{h,\mathbf{n}}$ on fractures F2–F4 (see Figure 6.6(b)). As we refine the mesh, we expect the approximate mean to converge to the exact mean; both schemes identify, at convergence, the same value for F2, F3, and F4, but the high-order scheme already gives this value on the coarsest meshes, and with fewer degrees of freedom than the low-order scheme. A comparison of the Newton iteration counts required to reach a tolerance of 10^{-12} for the lowest-order method [32], and the present scheme is reported in Table 6.2. Furthermore, Figure 6.7 demonstrates that the discrete normal traction produced by the current scheme is considerably smoother than that obtained with the lowest-order approach [32]. This establishes the higher-order scheme as both more accurate and computationally efficient. This advantage extends to fracture F1, where the higher-order method yields a more accurate mean normal displacement jump (Figure 6.8(a)) and a superior resolution of the contact transition zone (Figure 6.6(a)), as evidenced by the more precise mean $\lambda_{h,\mathbf{n}}$ profile in Figure 6.8(b).

	Mesh	1	2	3	4	5
Lowest-order method [32]	Nb Newton iterations	12	12	12	12	13
	Degrees of Freedom	4092	20592	52665	85566	127047
Present method	Nb Newton iterations	5	7	7	7	7
	Degrees of Freedom	32463	205515	609507	1087011	1703745

Table 6.2: Test case from Section 6.4: Comparison between the lowest-order method [32] and the current higher-order scheme on the number of Newton iterations required to converge within the desired tolerance of 10^{-12} .

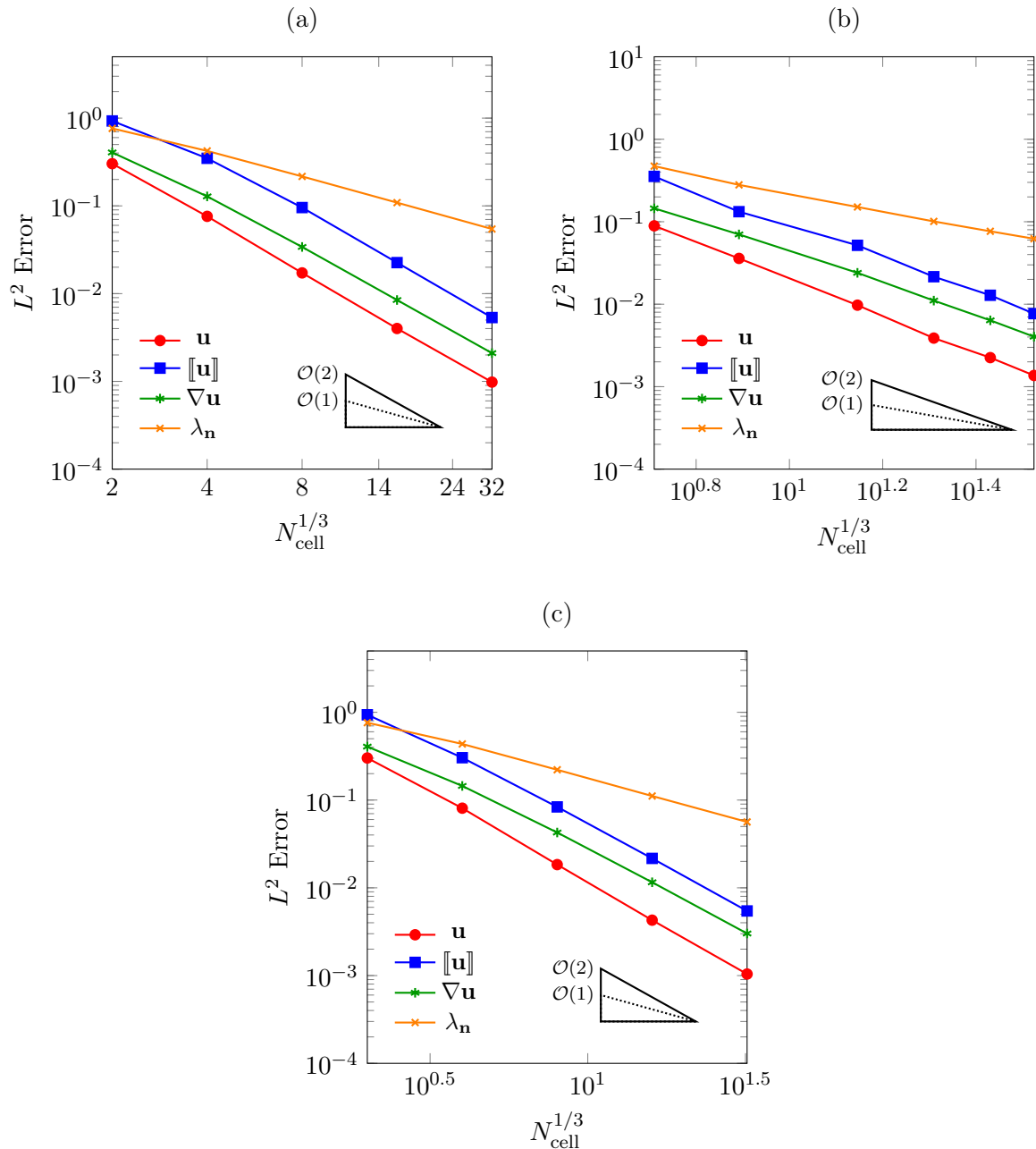


Figure 6.1: (Test case from Section 6.1). Relative L^2 -norm of errors $\mathbf{u} - \Upsilon_h^2(\mathbf{u}_h)$, $[\mathbf{u}] - [[\mathbf{u}_h]]_h$, $\nabla \mathbf{u} - \nabla \Upsilon_h^2(\mathbf{u}_h)$, and $\lambda_{\mathbf{n}} - \lambda_{h,\mathbf{n}}$ versus the cubic root of the number of cells, for (a) Cartesian, (b) tetrahedral, and (c) Hexa-cut mesh families.

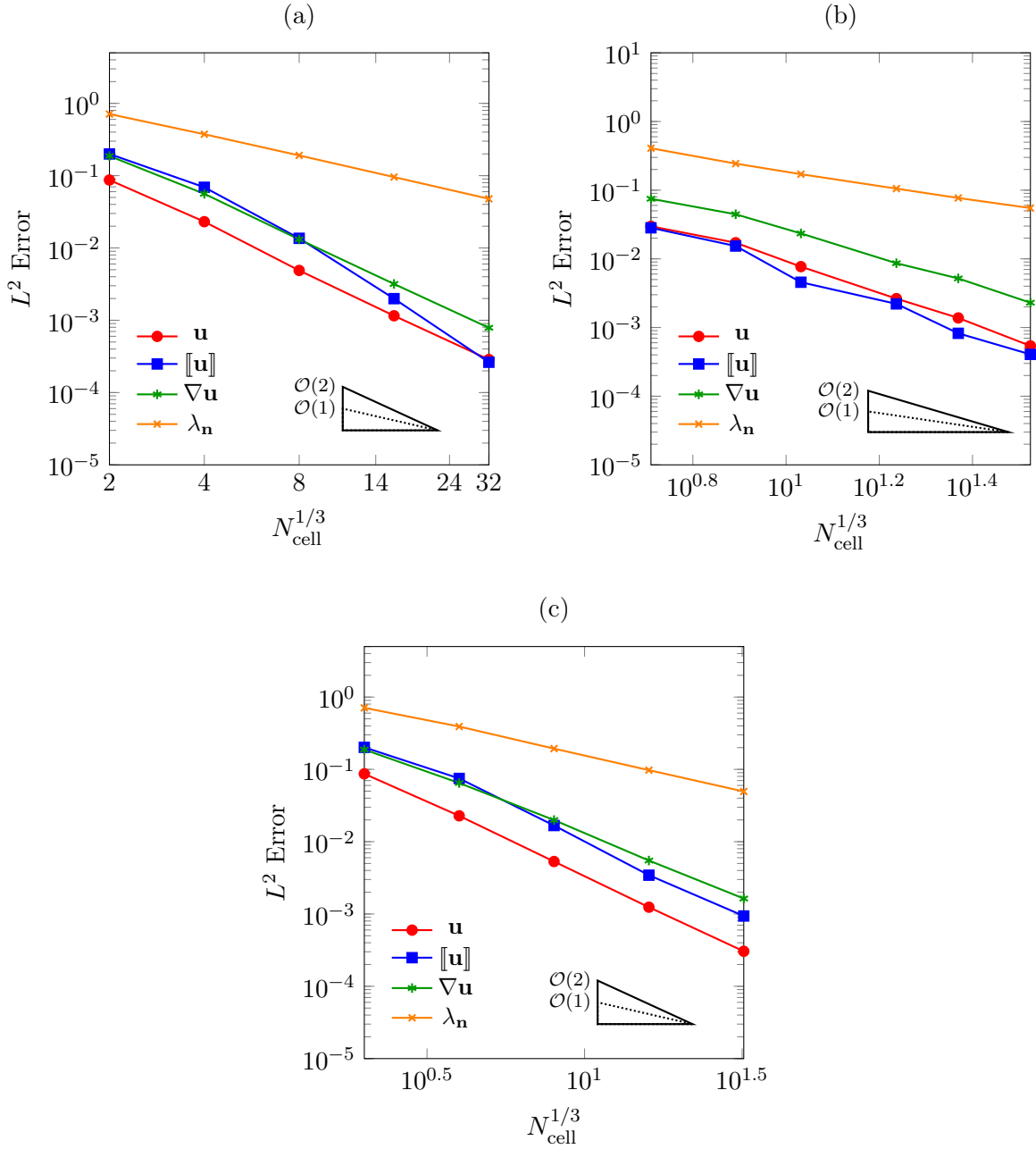


Figure 6.2: (Test case from Section 6.2). Relative L^2 -norm errors of $\mathbf{u} - \Upsilon_h^2(\mathbf{u}_h)$, $[\mathbf{u}] - [\mathbf{u}_h]_h$, $\nabla \mathbf{u} - \nabla \Upsilon_h^2(\mathbf{u}_h)$, and $\lambda_n - \lambda_{h,n}$ versus the cubic root of the number of cells, for (a) Cartesian, (b) tetrahedral, and (c) Hexa-cut mesh families.

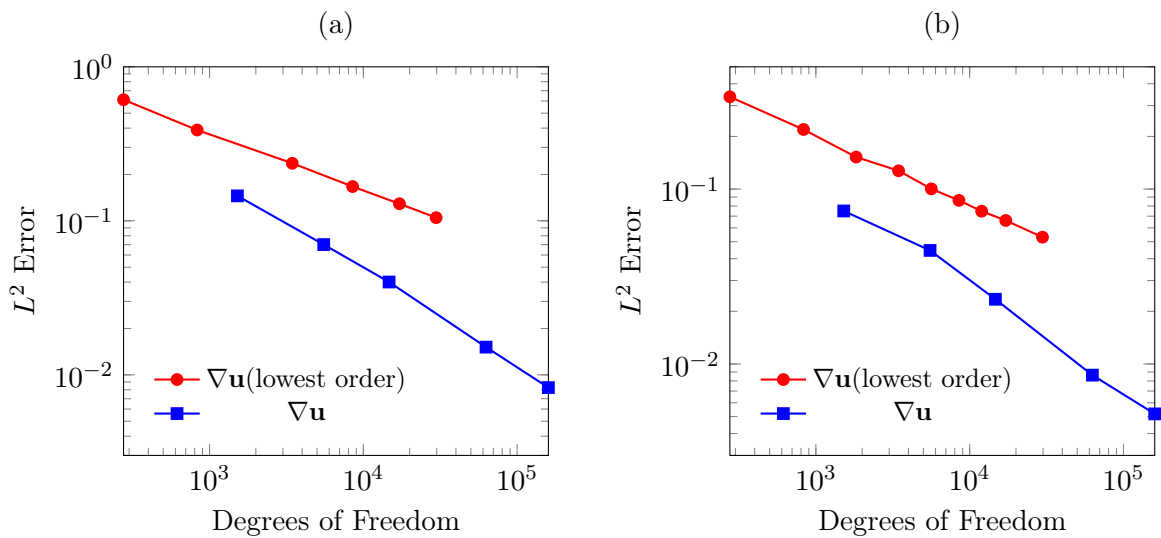


Figure 6.3: ((a) Test case from Section 6.1 and (b) Test case from Section 6.2). Comparison of L^2 -norm of $\nabla \mathbf{u} - \nabla \Upsilon_h^2(\underline{\mathbf{u}}_h)$ of the lowest-order method [32] with the current higher-order scheme for a tetrahedral mesh.

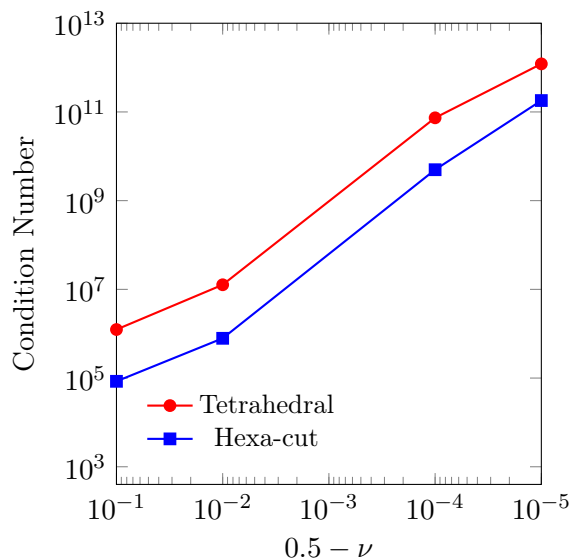


Figure 6.4: Condition number vs ν . Test case of Section 6.3.

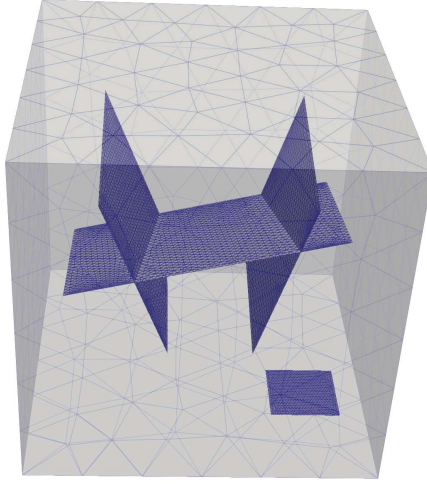


Figure 6.5: Fracture network for the test case in Section 6.4

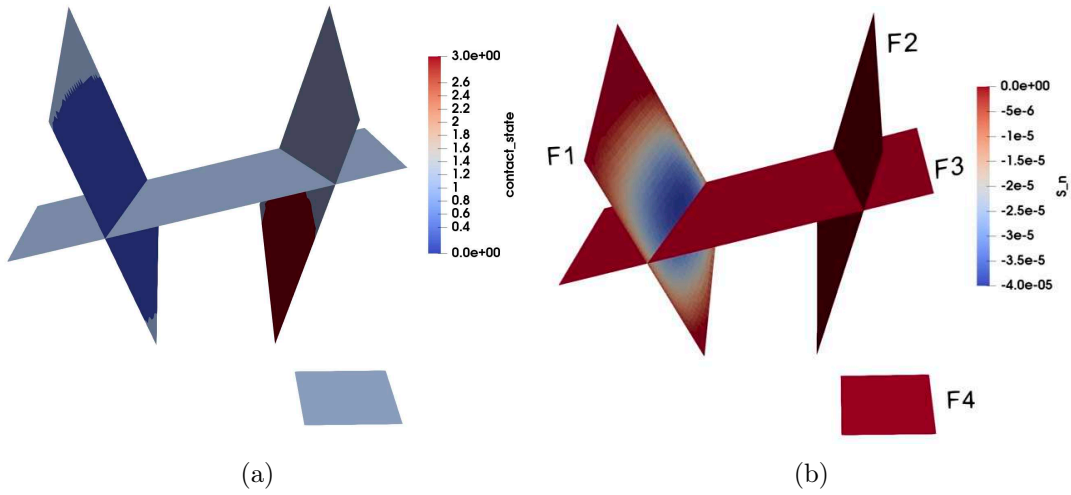


Figure 6.6: Results for the test case in Section 6.4: (a) contact state classification, where the values indicate: 0 if $|\lambda_{h,\tau}| < g$ and $[[\mathbf{u}_h]]_{h,\mathbf{n}} < 0$; 1 if $|\lambda_{h,\tau}| < g$ and $[[\mathbf{u}_h]]_{h,\mathbf{n}} = 0$; 2 if $|\lambda_{h,\tau}| = g$ and $[[\mathbf{u}_h]]_{h,\mathbf{n}} < 0$; and 3 if $|\lambda_{h,\tau}| = g$ and $[[\mathbf{u}_h]]_{h,\mathbf{n}} = 0$; and (b) normal displacement jump obtained using the DDR discretisation with 123k cells and 8.8k fracture faces.

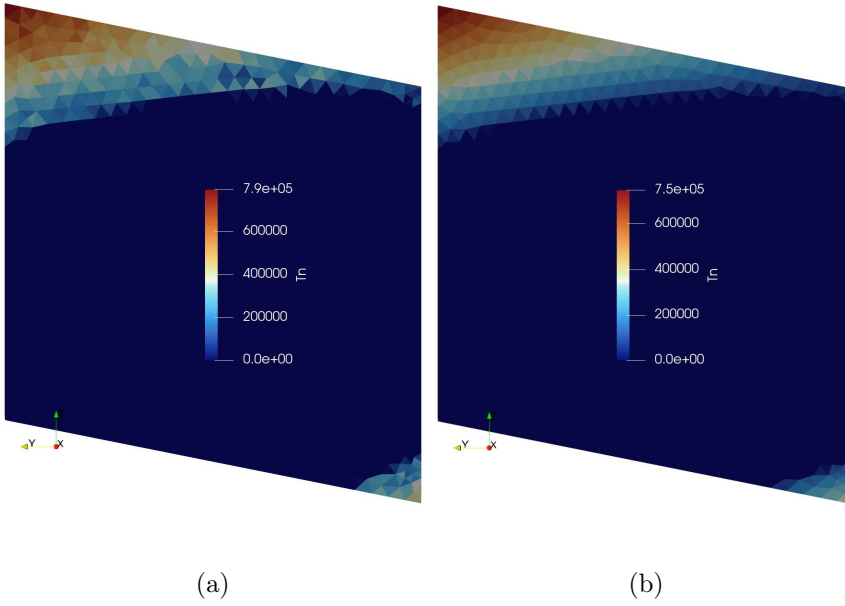


Figure 6.7: Test case from Section 6.4: Plot of normal component of discrete Lagrange multiplier: (a) lowest-order method [32] and (b) the current higher-order scheme for fracture F1 on a tetrahedral mesh.

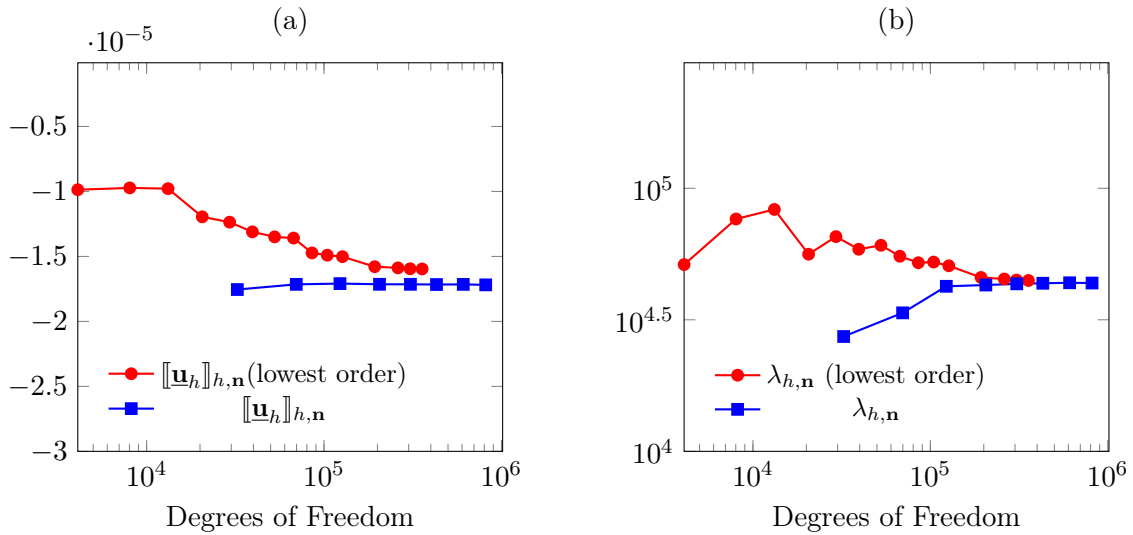


Figure 6.8: Test case from Section 6.4: Comparison between the lowest-order method [32] and the current higher-order scheme for fracture F1 on a tetrahedral mesh: (a) Mean value of normal displacement jump and (b) Mean value of normal component of the discrete Lagrange multiplier.

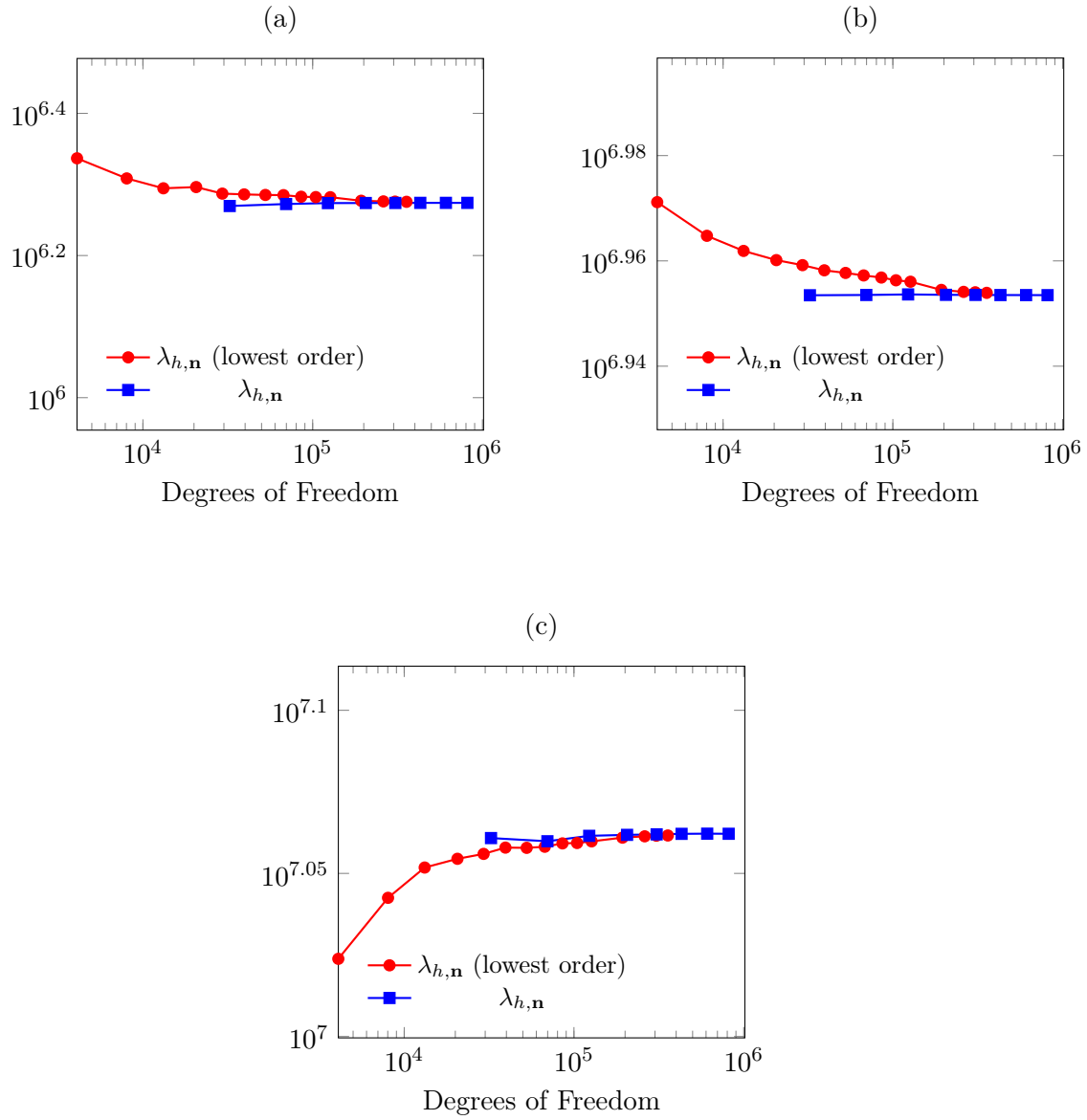


Figure 6.9: Test case from Section 6.4: Mean value of normal component of the discrete Lagrange multiplier for fractures F2, F3, and F4 are shown in (a), (b), and (c), respectively. Results compare the lowest-order method [32] with the current higher-order scheme on a tetrahedral mesh.

Acknowledgments

We acknowledge the funding of the European Union via the ERC Synergy, NEMESIS, project number 101115663. Views and opinions expressed are, however, those of the authors only and do not necessarily reflect those of the European Union or the European Research Council Executive Agency. Neither the European Union nor the granting authority can be held responsible for them.

References

- [1] F. Abbassi, A. Karrech, M.S. Islam, and A. C. Seibi. Poromechanics of fractured/faulted reservoirs during fluid injection based on continuum damage modeling and machine learning. *Natural Resources Research*, 32(1):413–430, 2023.
- [2] P. Alart and A. Curnier. A mixed formulation for frictional contact problems prone to newton like solution methods. *Computer Methods in Applied Mechanics and Engineering*, 92(3):353–375, 1991.
- [3] C. Alboin, J. Jaffre, J. Roberts, and C. Serres. Modeling fractures as interfaces for flow and transport in porous media. *Fluid flow and transport in porous media*, 295:13–24, 2002.
- [4] D. Arnold. *Finite Element Exterior Calculus*. SIAM, 2018.
- [5] L. Beirão Da Veiga, F. Brezzi, and L.D. Marini. Virtual elements for linear elasticity problems. *SIAM Journal on Numerical Analysis*, 51:794–812, 2013.
- [6] F. Ben Belgacem and Y. Renard. Hybrid finite element methods for the Signorini problem. *Mathematics of Computation*, 72(243):1117–1145, 2003.
- [7] R. L. Berge, I. Berre, E. Keilegavlen, J. M. Nordbotten, and B. Wohlmuth. Finite volume discretization for poroelastic media with fractures modeled by contact mechanics. *International Journal for Numerical Methods in Engineering*, 121:644–663, 2019.
- [8] F. Bonaldi, K. Brenner, J. Droniou, and R. Masson. Gradient discretization of two-phase flows coupled with mechanical deformation in fractured porous media. *Computers and Mathematics with Applications*, 98:40–68, 2021.
- [9] F. Bonaldi, J. Droniou, R. Masson, and A. Pasteau. Energy-stable discretization of two-phase flows in deformable porous media with frictional contact at matrix-fracture interfaces. *Journal of Computational Physics*, 455:Paper No. 110984, 28, 2022.
- [10] Francesco Bonaldi, Konstantin Brenner, Jérôme Droniou, Roland Masson, Antoine Pasteau, and Laurent Trenty. Gradient discretization of two-phase poro-mechanical models with discontinuous pressures at matrix fracture interfaces. *ESAIM: M2AN*, 55(5):1741–1777, 2021.
- [11] S.C. Brenner and L.R. Scott. *The Mathematical Theory of Finite Element Methods*. Springer, 2008.
- [12] F. Brezzi and M. Fortin. *Mixed and hybrid finite element methods*. Springer New York, NY, 1991.
- [13] F. Chouly, P. Hild, V. Lleras, and Y. Renard. Nitsche method for contact with Coulomb friction: existence results for the static and dynamic finite element formulations. 2020.

- [14] F. Chouly, P. Hild, and Y. Renard. *Finite Element Approximation of Contact and Friction in Elasticity*. Birkhäuser Cham, 2023.
- [15] Franz Chouly. An adaptation of nitsche’s method to the tresca friction problem. *Journal of Mathematical Analysis and Applications*, 411(1):329–339, 2014.
- [16] Franz Chouly, Alexandre Ern, and Nicolas Pignet. A hybrid high-order discretization combined with nitsche’s method for contact and tresca friction in small strain elasticity. *SIAM Journal on Scientific Computing*, 42(4):A2300–A2324, 2020.
- [17] Franz Chouly, Alexandre Ern, and Nicolas Pignet. A hybrid high-order discretization combined with nitsche’s method for contact and tresca friction in small strain elasticity. *SIAM Journal on Scientific Computing*, 42(4):A2300–A2324, 2020.
- [18] M. Cihan, B. Hudobivnik, J. Korelc, and P. Wriggers. A virtual element method for 3d contact problems with non-conforming meshes. *Computer Methods in Applied Mechanics and Engineering*, 402:115385, 2022. A Special Issue in Honor of the Lifetime Achievements of J. Tinsley Oden.
- [19] Monique Dauge. *Elliptic Boundary Value Problems on Corner Domains*, volume 1341 of *Lecture Notes in Mathematics*. Springer, 1988.
- [20] D. Di Pietro and A. Ern. A hybrid high-order locking-free method for linear elasticity on general meshes. *Computer Methods in Applied Mechanics and Engineering*, 283:1–21, 2015.
- [21] D. A. Di Pietro, J. Droniou, and J. J. Qian. A pressure-robust Discrete de Rham scheme for the Navier–Stokes equations. *Comput. Meth. Appl. Mech. Engrg.*, 421(116765), 2024.
- [22] Daniele A. Di Pietro and Jérôme Droniou. A discrete de rham method for the reissner–mindlin plate bending problem on polygonal meshes. *Comput. Math. Appl.*, 125(C):136–149, November 2022.
- [23] Daniele A. Di Pietro and Jérôme Droniou. A fully discrete plates complex on polygonal meshes with application to the Kirchhoff–Love problem. *Math. Comp.*, 92:51–77, 2023.
- [24] Daniele A. Di Pietro, Jérôme Droniou, and Francesca Rapetti. Fully discrete polynomial de rham sequences of arbitrary degree on polygons and polyhedra. *Math. Models Methods Appl. Sci.*, 30(9):1809–1855, 2020.
- [25] Daniele Antonio Di Pietro and Jérôme Droniou. *The Hybrid High-Order Method for Polytopal Meshes: Design, Analysis, and Applications*, volume 19 of *Modeling, Simulation and Applications*. Springer International Publishing, 2020.
- [26] Daniele Antonio Di Pietro and Jérôme Droniou. An arbitrary-order discrete de rham complex on polyhedral meshes: Exactness, poincaré inequalities, and consistency. *Foundations of Computational Mathematics*, pages 1–80, 2021.
- [27] Zhaonan Dong and Alexandre Ern. Hybrid high-order and weak galerkin methods for the biharmonic problem. *SIAM Journal on Numerical Analysis*, 60(5):2626–2656, 2022.
- [28] J. Droniou, R. Eymard, T. Gallouët, C. Guichard, and R. Herbin. *The Gradient Discretisation Method*, volume 82 of *Mathematics & Applications*. Springer, 2018.
- [29] J. Droniou, M. Hanot, and T. A. Oliynyk. A polytopal discrete de rham complex on manifolds, with application to the maxwell equations. *Journal of Computational Physics*, 529:113886, 2025.

- [30] J Droniou, T. A. Oliynyk, and J. J. Qian. A polyhedral discrete de rham numerical scheme for the yang-mills equations. *Journal of Computational Physics*, 478:111955, 2023.
- [31] Jérôme Droniou, Guillaume Enchéry, Isabelle Faille, Ali Haidar, and Roland Masson. A bubble vem–fully discrete polytopal scheme for mixed-dimensional poromechanics with frictional contact at matrix-fracture interfaces. *Computer Methods in Applied Mechanics and Engineering*, 422:116838, 2024.
- [32] Jérôme Droniou, Ali Haidar, and Roland Masson. Analysis of a vem–fully discrete polytopal scheme with bubble stabilisation for contact mechanics with tresca friction. *M2AN Math. Model. Numer. Anal.*, page 31p, 2025.
- [33] Guillaume Drouet and Patrick Hild. Optimal convergence for discrete variational inequalities modelling Signorini contact in 2D and 3D without additional assumptions on the unknown contact set. *SIAM J. Numer. Anal.*, 53(3):1488–1507, 2015.
- [34] A. Franceschini, N. Castelletto, J.A. White, and H.A. Tchelepi. Algebraically stabilized Lagrange multiplier method for frictional contact mechanics with hydraulically active fractures. *Computer Methods in Applied Mechanics and Engineering*, 368:113161, 2020.
- [35] T. T. Garipov and M. H. Hui. Discrete fracture modeling approach for simulating coupled thermo-hydro-mechanical effects in fractured reservoirs. *International Journal of Rock Mechanics and Mining Sciences*, 122:104075, 2019.
- [36] T. T. Garipov, M. Karimi-Fard, and H.A. Tchelepi. Discrete fracture model for coupled flow and geomechanics. *Computational Geosciences*, 20(1):149–160, 2016.
- [37] Christophe Geuzaine and Jean-François Remacle. Gmsh: A 3-d finite element mesh generator with built-in pre- and post-processing facilities. *International Journal for Numerical Methods in Engineering*, 79(11):1309–1331, 2009.
- [38] P. Hansbo and M.G. Larson. Discontinuous galerkin and the crouzeix–raviart element: Application to elasticity. *ESAIM: Mathematical Modelling and Numerical Analysis*, 37:63–72, 2003.
- [39] J. Haslinger, I. Hlaváček, and J. Necas. Numerical methods for unilateral problems in solid mechanics. In *Finite Element Methods (Part 2), Numerical Methods for Solids (Part 2)*, volume 4 of *Handbook of Numerical Analysis*, pages 313–485. Elsevier, 1996.
- [40] Patrick Hild and Yves Renard. An error estimate for the signorini problem with coulomb friction approximated by finite elements. *SIAM Journal on Numerical Analysis*, 45(5):2012–2031, 2007.
- [41] Mohamed Laaziri and Roland Masson. Vem fully discrete nitsche’s discretization of coulomb frictional contact-mechanics for mixed-dimensional poromechanical models. *Computational Geosciences*, 29(6):50, 2025.
- [42] Mohamed Laaziri and Roland Masson. Vem-nitsche fully discrete polytopal scheme for frictionless contact-mechanics. *SIAM Journal on Numerical Analysis*, 63(1):81–102, 2025.
- [43] V. Martin, J. Jaffré, and J. E. Roberts. Modeling fractures and barriers as interfaces for flow in porous media. *SIAM Journal on Scientific Computing*, 26:1667–1691, 2005.
- [44] Morteza Nejati, Adriana Paluszny, and Robert W. Zimmerman. A finite element framework for modeling internal frictional contact in three-dimensional fractured media using

unstructured tetrahedral meshes. *Computer Methods in Applied Mechanics and Engineering*, 306:123–150, 2016.

- [45] B. I. Wohlmuth, A. Popp, M. W. Gee, and W. A. Wall. An abstract framework for a priori estimates for contact problems in 3D with quadratic finite elements. *Comput. Mech.*, 49(6):735–747, 2012.
- [46] Bangmin Wu, Fei Wang, and Weimin Han. Virtual element method for a frictional contact problem with normal compliance. *Communications in Nonlinear Science and Numerical Simulation*, 107:106125, 2022.